


Article

Synthesis, Structure, and Magnetic Properties of Linear Trinuclear Cu^{II} and Ni^{II} Complexes of Porphyrin Analogues Embedded with Binaphthol Units

Jun-ichiro Setsune ^{1,*}, Shintaro Omae ¹, Yukinori Tsujimura ¹, Tomoyuki Mochida ¹, Takahiro Sakurai ² and Hitoshi Ohta ³

¹ Department of Chemistry, Graduate School of Science, Kobe University, Hyogo 657-8501, Japan; 092s208s@stu.kobe-u.ac.jp (S.O.); 119s217s@stu.kobe-u.ac.jp (Y.T.); tmochida@platinum.kobe-u.ac.jp (T.M.)

² Research Facility Center for Science and Technology, Kobe University, Hyogo 657-8501, Japan; tsakurai@kobe-u.ac.jp

³ Molecular Photoscience Research Center, Kobe University, Hyogo 657-8501, Japan; hohta@kobe-u.ac.jp

* Correspondence: setsunej@kobe-u.ac.jp

Received: 26 August 2020; Accepted: 24 September 2020; Published: 28 September 2020



Abstract: A porphyrin analogue embedded with (*S*)-1,1'-bi-2-naphthol units was synthesized without reducing optical purity of the original binaphthol unit. This new macrocyclic ligand provides the hexaanionic N₄O₄ coordination environment that enables a linear array of three metal ions. That is, it provides the square planar O₄ donor set for the central metal site and the distorted square planar N₂O₂ donor set for the terminal metal sites. In fact, a Cu^{II}₃ complex with a Cu(1)–Cu(2) distance of 2.910 Å, a Cu(1)–Cu(2)–Cu(1') angle of 174.7°, and a very planar Cu₂O₂ diamond core was obtained. The variable-temperature ¹H-NMR study of the Cu^{II}₃ complex showed increasing paramagnetic shifts for the naphthyl protons as temperature increased, which suggests strong antiferromagnetic coupling of Cu^{II} ions. The temperature dependence of the magnetic susceptibility indicated antiferromagnetic coupling both for the Cu^{II}₃ complex ($J = -434 \text{ cm}^{-1}$) and for the Ni^{II}₃ complex ($J = -49 \text{ cm}^{-1}$). The linear (L)M(μ-OR)₂M(μ-OR)₂M(L) core in a rigid macrocycle cavity made of aromatic components provides robust metal complexes that undergo reversible ligation at the apical sites of the central metal.

Keywords: porphyrinoids; multinuclear complexes; chiral ligands; circular dichroism; paramagnetic NMR; magnetochemistry

1. Introduction

Porphyrin analogues provide well-preorganized metal sites due to their rigid molecular structure made of aromatic building blocks with extended π -electron delocalization. In particular, the coordination chemistry of porphyrin analogues of a large ring size has extensively been studied and a number of multinuclear metal complexes have been generated [1–3]. Ligands for supporting multimetallic units in a designed arrangement of metals are of great importance because an unusual electronic structure and reactivity are expected for such metal assemblies. In fact, the magnetochemistry of dinuclear Cu^{II} complexes of such porphyrin analogues has been studied extensively, and the catalytic activity of dinuclear Co complexes has been reported [4–10]. However, examples of trinuclear and tetranuclear complexes of porphyrin analogues are still quite limited [11–17]. It is well known that two parts of mononuclear complexes such as (L)M(OR)₂ are bridged by the third metal to give trinuclear complexes (L)M(μ-OR)₂M(μ-OR)₂M(L), where three metals are assembled in a linear array by the multiple μ -alkoxy bridges to generate a M₃O₄ core with strong metal–metal interaction [18–30]. These complexes are not

so stable because of the relatively weak ligation to the central metal, in addition to the steric repulsion between two mononuclear complexes. Inclusion of such trinuclear units inside a large macrocycle would improve their stability against decomposition, which is helpful to gain further insight into the properties and reaction behaviors of trinuclear complexes. Examples of linear trinuclear Cu^{II} complexes of macrocyclic ligands are not abundant [31–33]. For example, the trinuclear Cu^{II} complex **A** of an octaazacryptand ligand was recently reported [32] (Figure 1).

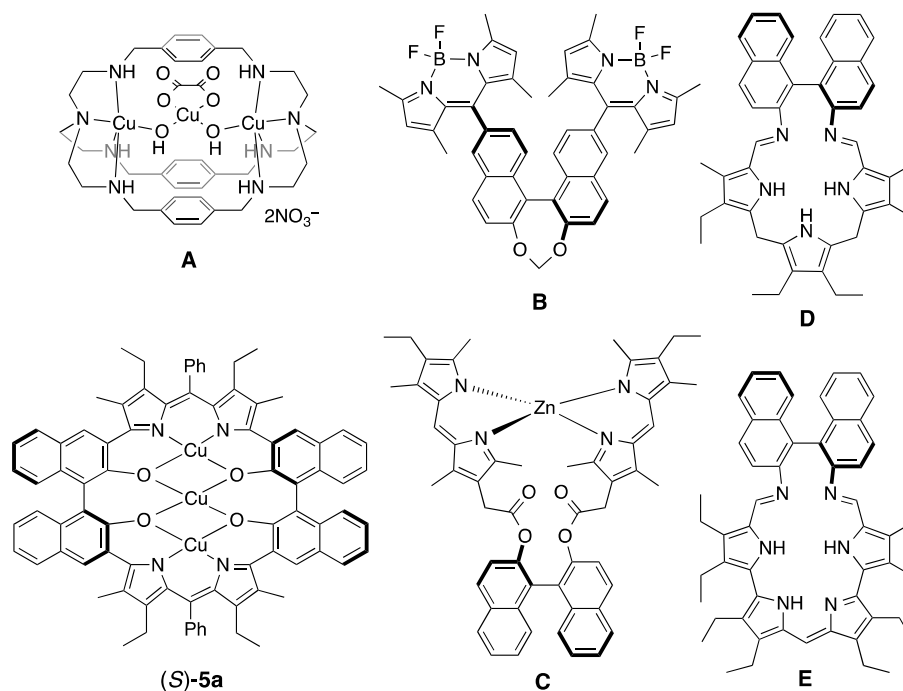
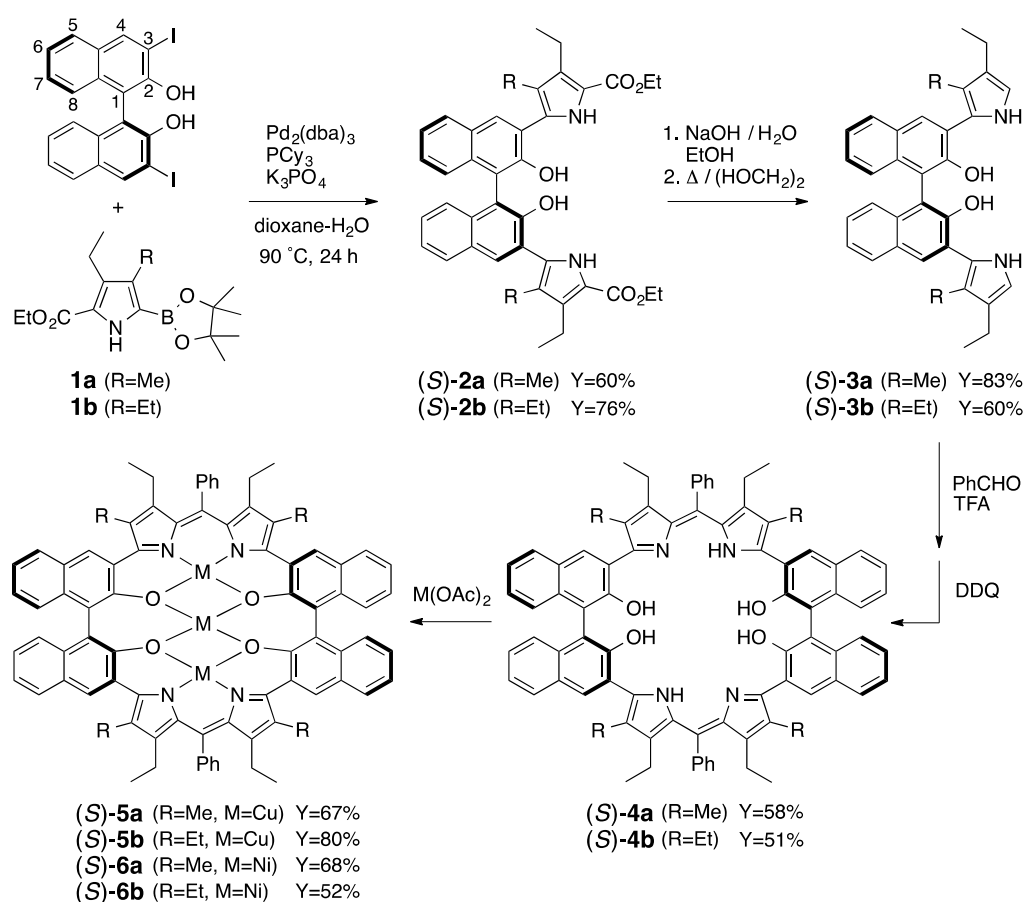


Figure 1. The reported trinuclear metal complexes (**A** and **(S)-5a**) of macrocyclic ligands and 1,1'-binaphthyl dipyrroin conjugates (**B–E**).

When a dipyrroin unit and a 1,1'-binaphthyl unit are combined, such hybrid molecules can generate metal complexes with interesting chiroptical properties (Figure 1). In the reported compounds, **B** and **C**, the 1,1'-binaphthyl unit was substituted with dipyrroin boron complexes and a bisdipyrroin zinc complex, respectively [34,35]. Compound **C** is a highly diastereoselective (>99% d.r.) helicate, and compound **B** showed redox-induced switching of the chiroptical signal. Macrocycles, **D** and **E**, were prepared via the condensation of tri- and tetrapyrrolic dialdehydes with 1,1'-binaphthyl-2,2'-diamine, and they contain the chiral atropisomeric 1,1'-binaphthyl substructure as a part of the ring system [36]. However, these macrocycles have never been studied extensively. It is also noteworthy that enantioselective recognition of carboxylate anions was achieved by chiral calix[4]pyrroles bearing an (*R*)- or (*S*)-1,1'-bi-2-naphthol strap [37]. We previously developed a stable and relatively rigid macrocycle with direct bonding between the binaphthyl ring carbon and the pyrrole ring carbon through a cross-coupling reaction, where four hydroxy groups and two dipyrroins are preorganized to support a linear trinuclear metal system [17]. In that preliminary communication, we reported the X-ray crystal structure of the tricopper complex **(S)-5a** and showed reversible coordination of the amine to the apical site of the central Cu ion (Figure 1). Here, we describe the chemistry of the trinuclear metal complexes of these porphyrinoid ligands embedded with binaphthol units in detail, including previous results of the X-ray structure and coordination chemistry of **(S)-5a**. We synthesized an analogous Cu^{II}_3 complex **(S)-5b** having different alkyl substituents at the macrocycle core from those in **(S)-5a**, and the corresponding Ni^{II}_3 complexes, **(S)-6a** and **(S)-6b**, were also prepared (Scheme 1). In particular, the magnetic properties of these Cu^{II}_3 and Ni^{II}_3 complexes are discussed extensively on the basis of paramagnetic $^1\text{H-NMR}$ in solution and magnetic susceptibility in solid state.



Scheme 1. Synthesis of binaphthol-embedded porphyrin analogues. Atom numberings in the 1,1'-binaphthyl unit shown in **1a** and **1b** are applied to all compounds.

2. Materials and Methods

General: A Varian Inova 400 spectrometer (400 MHz) was used for the $^1\text{H-NMR}$ measurement. Chemical shifts were recorded against $(\text{CH}_3)_4\text{Si}$ (0 ppm) as an internal standard. The ultraviolet (UV)-visible and circular dichroism (CD) spectra were measured on a JASCO V-570 spectrometer and J-820F spectropolarimeter, respectively. A YANACO MT-5 CHN recorder was employed for elemental analyses. An Applied Biosystems Mariner mass spectrometer was used for the measurement of electrospray ionization (ESI) time-of-flight (TOF) MS spectra.

5-Carboethoxy-4-ethyl-3-methyl-2-(4,4,5,5-tetramethyl-1,3,2-dioxaborolan-2-yl)pyrrole

(2-Borylpyrrole) (1a): a tetrahydrofuran (THF) solution (6 mL) of 5-carboethoxy-4-ethyl-3-methyl-2-iodopyrrole (470 mg, 1.53 mmol), 4,4,5,5-tetramethyl-1,3,2-dioxaborolane (235 mg, 1.84 mmol), dichlorobis(triphenylphosphine)palladium(II) (17.4 mg, 0.025 mmol), and triethylamine (430 mg, 4.26 mmol) was refluxed gently with stirring for 2 h under argon. The reaction mixture was evaporated under vacuum and then hexane was added to the residue. The formed precipitate was filtered off and the filtrate was evaporated to give the oily substance in almost quantitative yield. This 2-borylpyrrole was used for the cross-coupling reaction without further purification. $^1\text{H-NMR}$ (400 MHz, δ -value in CDCl_3) 9.08 (broad s, 1H, NH); 4.32 (q, 2H, $J = 7.1$ Hz, OCH_2Me); 2.74 (q, 2H, $J = 7.3$ Hz, CH_2Me); 2.21 (s, 3H, pyrrole β -Me); 1.35 (t, 3H, $J = 7.1$ Hz, OCH_2Me); 1.30 (s, 12H, dioxaborolane-Me); 1.11 (t, 3H, $J = 7.3$ Hz, pyrrole β - CH_2Me). ESI-MS 308.24/308.20 (found/calculated for $(\text{C}_{16}\text{H}_{26}\text{BNO}_4 (\text{M}) + \text{H})^+$).

5-Carboethoxy-3,4-diethyl-2-(4,4,5,5-tetramethyl-1,3,2-dioxaborolan-2-yl)pyrrole

(2-Borylpyrrole) (1b): This compound was prepared from 5-carboethoxy-3,4-diethyl-2-iodopyrrole according to the procedure for **1a** [38,39]. $^1\text{H-NMR}$ (400 MHz, δ -value, CDCl_3) 9.17 (broad s, 1H, NH), 4.32 (q, 2H, $J = 7.2$ Hz, OCH_2Me), 2.75 and 2.65 (2q, 4H, $J = 7.5$ and 7.5 Hz, pyrrole β - CH_2Me), 1.36 (t,

3H, $J = 7.2$ Hz, OCH_2Me), 1.30 (s, 12H, dioxoborolane-Me), 1.15 and 1.13 (2t, 6H, $J = 7.5$ and 7.5 Hz, pyrrole $\beta\text{-CH}_2\text{Me}$).

(S)-3,3'-Bis(5-carboethoxy-4-ethyl-3-methyl-2-pyrrolyl)-1,1'-bi-2-naphthol ((S)-2a): To a mixture of (S)-3,3'-diiodo-1,1'-bi-2-naphthol (345 mg, 0.64 mmol), 5-carboethoxy-4-ethyl-3-methyl-2-(4,4,5,5-tetramethyl-1,3,2-dioxaborolan-2-yl)pyrrole (**1a**) (ca. 1.5 mmol), tris(dibenzylideneacetone) dipalladium (60.4 mg, 0.066 mmol), and tricyclohexylphosphine (40.2 mg, 0.14 mmol), an aqueous solution (1.2 mL) of potassium phosphate tribasic (430 mg, 2.0 mmol) and dioxane (6 mL) was added. The reaction mixture was heated at 90–100 °C with stirring under argon for 24 h. After cooling, the reaction mixture was partitioned between CH_2Cl_2 and water. The organic products were extracted from the water layer with CH_2Cl_2 . The combined organic layer was dried over anhydrous Na_2SO_4 and then evaporated to dryness under vacuum. The residue dissolved in acetone was passed through a silica gel column. This acetone solution was evaporated and then crystallized from methanol to afford white powders (248 mg) of the cross-coupling product. Yield 60%. $^1\text{H-NMR}$ (400 MHz, δ -value in CDCl_3) 9.60 (broad s, 2H, NH); 8.16 (broad s, 2H, 1,1'-binaphthyl-4,4'-H); 7.93 and 7.17 (2 broad signals, 4H, 1,1'-binaphthyl-5,5',8,8'-H); 7.42 and 7.32 (2 broad signals, 4H, 1,1'-binaphthyl-6,6',7,7'-H); 5.59 (broad s, 2H, OH); 4.28 (broad signal, 4H, OCH_2Me); 2.87 (broad signal, 4H, pyrrole $\beta\text{-CH}_2\text{Me}$); 2.33 (s, 6H, pyrrole $\beta\text{-Me}$); 1.32 (broad signal, 6H, OCH_2Me); 1.20 (t, 6H, $J = 7.5$ Hz, pyrrole $\beta\text{-CH}_2\text{Me}$). ESI-MS 667.27/667.27 (found/calculated for $(\text{C}_{40}\text{H}_{40}\text{N}_2\text{O}_6 (\text{M}) + \text{Na})^+$). Analysis calculated for $\text{C}_{40}\text{H}_{40}\text{N}_2\text{O}_6$: C, 74.50; H, 6.25; N, 4.34. Found: C, 73.94; H, 6.21; N, 4.27.

(S)-3,3'-Bis(5-carboethoxy-3,4-diethyl-2-pyrrolyl)-1,1'-bi-2-naphthol ((S)-2b): This compound was prepared from 5-carboethoxy-3,4-diethyl-2-(4,4,5,5-tetramethyl-1,3,2-dioxaborolan-2-yl)pyrrole (**1b**) according to the procedure for (S)-**2a**. Yield 76%. $^1\text{H-NMR}$ (400 MHz, δ -value in CDCl_3) 9.54 (broad s, 2H, NH); 8.14 (broad s, 2H, 1,1'-binaphthyl-4,4'-H); 7.91 and 7.16 (broad 2d, 4H, $J = 7.9$ and 8.3 Hz, 1,1'-binaphthyl-5,5',8,8'-H); 7.41 and 7.32 (2 broad signals, 4H, 1,1'-binaphthyl-6,6',7,7'-H); 5.60 (broad s, 2H, OH); 4.26 (broad signal, 4H, OCH_2Me); 2.83 and 2.72 (2 broad q, $J = 7.3$ and 7.3 Hz, 8H, pyrrole $\beta\text{-CH}_2\text{Me}$); 1.31 (broad signal, 6H, OCH_2Me); 1.27 and 1.24 (2t, 12H, $J = 7.3$ and 7.3 Hz, pyrrole $\beta\text{-CH}_2\text{Me}$). ESI-MS 673.33/673.32 (found/calculated for $(\text{C}_{42}\text{H}_{44}\text{N}_2\text{O}_6 (\text{M}) + \text{H})^+$). Analysis calculated for $\text{C}_{42}\text{H}_{44}\text{N}_2\text{O}_6$: C, 74.98; H, 6.59; N, 4.16. Found: C, 75.13; H, 6.35; N, 3.79.

(S)-3,3'-Bis(4-ethyl-3-methyl-2-pyrrolyl)-1,1'-bi-2-naphthol ((S)-3a): A mixture of (S)-3,3'-bis(5-carboethoxy-4-ethyl-3-methyl-2-pyrrolyl)-1,1'-bi-2-naphthol ((S)-**2a**) (980 mg, 1.48 mmol), NaOH (950 mg, 23.8 mmol), ethanol (13 mL), dioxane (13 mL), and water (6.5 mL) was heated with stirring at 80 °C for 5 h under argon. After cooling, 5N HCl (6 mL) was added dropwise. The formed precipitates were filtered, washed with water, and then dried. To this carboxylic acid was then added ethylene glycol (20 mL), and the mixture was heated at 160 °C for 2 h under argon. Water was added to the cooled solution to form gray powders. The formed precipitates were filtered, washed with water, and then dried to give 553 mg of the product. Yield 83%. $^1\text{H-NMR}$ (400 MHz, δ -value in CDCl_3) 8.92 (broad s, 2H, NH); 8.10 (s, 2H, 1,1'-binaphthyl-4,4'-H); 7.90 and 7.15 (2 broad d, 4H, $J = 8.1$ and 8.3 Hz, 1,1'-binaphthyl-5,5',8,8'-H); 7.38 and 7.26 (2 broad t, 4H, 1,1'-binaphthyl-6,6',7,7'-H); 6.69 (s, 2H, pyrrole- α -H); 5.55 (broad s, 2H, OH); 2.55 (q, 4H, $J = 7.5$ Hz, pyrrole $\beta\text{-CH}_2\text{Me}$); 2.35 (s, 6H, pyrrole $\beta\text{-Me}$); 1.26 (t, 6H, $J = 7.5$ Hz, pyrrole $\beta\text{-CH}_2\text{Me}$). ESI-MS 501.30/501.25 (found/calculated for $(\text{C}_{34}\text{H}_{32}\text{N}_2\text{O}_2 (\text{M}) + \text{H})^+$). Analysis calculated for $\text{C}_{34}\text{H}_{32}\text{N}_2\text{O}_2$: C, 81.57; H, 6.44; N, 5.60. Found: C, 81.04; H, 6.28; N, 5.44.

(S)-3,3'-Bis(3,4-diethyl-2-pyrrolyl)-1,1'-bi-2-naphthol ((S)-3b): This compound was prepared from (S)-3,3'-bis(5-carboethoxy-3,4-diethyl-2-pyrrolyl)-1,1'-bi-2-naphthol (S)-**2b** according to the procedure for (S)-**3a**. Yield 60%. $^1\text{H-NMR}$ (400 MHz, δ -value in CDCl_3) 8.78 (broad s, 2H, NH); 8.07 (s, 2H, 1,1'-binaphthyl-4,4'-H); 7.89 and 7.15 (2 broad d, 4H, $J = 8.1$ and 8.3 Hz, 1,1'-binaphthyl-5,5',8,8'-H); 7.37 (ddd, 2H, $J = 8.1, 7.0, 1.2$ Hz, 1,1'-binaphthyl-6,6'- or -7,7'-H); 7.27 (ddd, 2H, $J = 8.3, 7.0, 1.2$ Hz, 1,1'-binaphthyl-6,6'- or -7,7'-H); 6.68 (s, 2H, pyrrole- α -H); 5.53 (broad s, 2H, OH); 2.74 and 2.58 (2q, 8H, $J = 7.6$ and 7.6 Hz, pyrrole $\beta\text{-CH}_2\text{Me}$); 1.30 and 1.28 (2t, 12H, $J = 7.6$ and 7.6 Hz, pyrrole $\beta\text{-CH}_2\text{Me}$). ESI-MS 559.25/560.30 (found/calculated for $(\text{C}_{36}\text{H}_{36}\text{N}_2\text{O}_2 (\text{M}) + \text{MeOH})^+$). Analysis calculated for

$C_{36}H_{36}N_2O_2$: C, 81.79; H, 6.86; N, 5.30; analysis calculated for $C_{36}H_{35}LiN_2O_2$: C, 80.88; H, 6.60; N, 5.24. Found: C, 80.98; H, 6.47; N, 5.11.

(S)-24,51-Diphenyl-22,26,49,53-tetraethyl-21,27,48,54-tetramethyl-57,58,61,62-tetrahydroxy-55,56,59,60-tetraaza-tridecacyclo(50,2,1,1^{2,10},0^{4,9},1^{11,19},0^{12,17},1^{20,23},1^{25,28},1^{29,37},0^{31,36},1^{38,46},0^{39,44},1^{47,50})dohexaconta-1(54),2(62),3,5,7,9,11,13,15,17,19(61),20(60),21,23,25,27,29(58),30,32,34,36,38,40,42,44,46(57),47(56),48,50,52-triacontaene ((S)-4a): To (S)-3,3'-bis(4-ethyl-3-methyl-2-pyrrolyl)-1,1'-bi-2-naphthol ((S)-3a) (127 mg, 0.25 mmol), dry CH_2Cl_2 (25 mL), trifluoroacetic acid (28.5 mg, 0.25 mmol), and benzaldehyde (40 mg, 0.38 mmol) were added under argon. After the mixture was stirred for 24 h at ambient temperature, 2,3-dichloro-5,6-dicyano-1,4-benzoquinone (DDQ) (133 mg, 0.59 mmol) was added. The reaction mixture was stirred for 2 h at ambient temperature. The resulting solution was washed with 2% aqueous $HClO_4$ solution, and then with 5% aqueous K_2CO_3 solution. The organic layer was dried over Na_2SO_4 , and then purified by column chromatography on silica gel. The purple fraction eluted with CH_2Cl_2 -acetone (10/1) was evaporated to dryness, and the residue was washed with methanol. Recrystallization from CH_2Cl_2 -hexane gave a purple powder (87 mg). Yield 58%. 1H -NMR (400 MHz, δ -value in $CDCl_3$) 8.34 (s, 4H, 1,1'-binaphthyl-4,4'-H); 7.80 and 7.00 (2 broad d, 8H, $J = 7.9$ and 8.3 Hz, 1,1'-binaphthyl-5,5',8,8'-H); 7.52 (m, 6H, phenyl-o,p-H); 7.43 (t, 4H, $J = 7.4$ Hz, phenyl-m-H); 7.24 and 7.16 (2 broad t, 8H, 1,1'-binaphthyl-6,6',7,7'-H); 2.43 (s, 12H, pyrrole β -Me); 1.87 and 1.65 (2m, 8H, pyrrole β - CH_2 Me); 0.74 (t, 12H, $J = 7.4$ Hz, pyrrole β - CH_2 Me). UV-vis (λ_{max} (log ϵ) in CH_2Cl_2) 347 (4.78), 553 (sh, 4.75), 572 (4.76). ESI-MS 1173.40/1173.53 (found/calculated for $(C_{82}H_{68}N_4O_4 (M) + H)^+$). Analysis calculated for $C_{82}H_{68}N_4O_4 \cdot 0.5(H_2O) \cdot (CH_2Cl_2)(C_6H_{14})$: C, 78.97; H, 6.33; N, 4.14. Found: C, 78.81; H, 6.28; N, 4.17.

(S)-24,51-Diphenyl-21,22,26,27,48,49,53,54-octaethyl-57,58,61,62-tetrahydroxy-55,56,59,60-tetraaza-tridecacyclo(50,2,1,1^{2,10},0^{4,9},1^{11,19},0^{12,17},1^{20,23},1^{25,28},1^{29,37},0^{31,36},1^{38,46},0^{39,44},1^{47,50})dohexaconta-1(54),2(62),3,5,7,9,11,13,15,17,19(61),20(60),21,23,25,27,29(58),30,32,34,36,38,40,42,44,46(57),47(56),48,50,52-triacontaene ((S)-4b): This compound was prepared from (S)-3,3'-bis(3,4-diethyl-2-pyrrolyl)-1,1'-bi-2-naphthol ((S)-3b) according to the procedure for (S)-4a. Yield 51%. 1H -NMR (400 MHz, δ -value, in $CDCl_3$) 8.35 (s, 4H, 1,1'-binaphthyl-4,4'-H); 7.79 and 7.00 (2 broad d, 8H, $J = 8.0$ and 8.3 Hz, 1,1'-binaphthyl-5,5',8,8'-H); 7.50 (m, 6H, phenyl-o,p-H); 7.42 (t, 4H, $J = 7.5$ Hz, phenyl-m-H); 7.24 (ddd, 4H, $J = 8.0, 6.9, 1.3$ Hz, 1,1'-binaphthyl-6,6'- or -7,7'-H); 7.17 (ddd, 4H, $J = 8.3, 6.9, 1.3$ Hz, 1,1'-binaphthyl-6,6'- or -7,7'-H); 2.89, 2.82, 1.96, and 1.54 (4m, 16H, pyrrole β - CH_2 Me); 1.36 and 0.74 (2t, 24H, $J = 7.4$ and 7.4 Hz, pyrrole β - CH_2 Me). UV-vis (λ_{max} (log ϵ) in CH_2Cl_2) 348 (4.85), 550 (sh, 4.78), 574 (4.79). ESI-MS 1229.59/1229.59 (found/calculated for $(C_{86}H_{76}N_4O_4 (M) + H)^+$). Analysis calculated for $C_{86}H_{76}N_4O_4$: C, 84.01; H, 6.23; N, 4.56. Found: C, 83.78; H, 6.05; N, 4.51.

Cu_3 complex ((S)-5a): A mixture of (S)-4a (18 mg, 0.015 mmol), $Cu(OAc)_2 \cdot 2H_2O$ (9.6 mg, 0.044 mmol), CH_2Cl_2 (4 mL), MeOH (3 mL), and triethylamine (20 mg, 0.2 mmol) was stirred for 5 h at ambient temperature. The color of the solution turned blue. After the solvent was removed under vacuum, column chromatography on silica gel with toluene as the eluent gave a blue fraction. Recrystallization from CH_2Cl_2 -MeOH afforded 13.8 mg of the Cu_3 complex. Yield 67%. 1H -NMR (400 MHz, δ -value, at 303 K in $CDCl_3$); 10.79, 7.99, 7.72, 6.80, 5.25 (5 broad signals, 20H, 1,1'-binaphthyl-4,4',5,5',7,7',6,6',8,8'-H); 9.61, 3.28 (2 broad signals, 8H, diastereotopic pyrrole β - CH_2 Me); 7.38 (broad signal, 2H, phenyl-p-H); 7.20 (broad signal, 4H, phenyl-m-H); 6.88 (broad signal, 4H, phenyl-o-H); 7.11 (broad signal, 12H, pyrrole β -Me); 0.98 (broad signal, 12H, pyrrole β - CH_2 Me). UV-vis (λ_{max} (log ϵ) in CH_2Cl_2) 354 (4.83), 418 (sh, 4.16), 582 (sh, 4.77), 617 (4.88), 635 (sh, 4.82). ESI-MS 1357.08/1357.26 (found/calculated for $(C_{82}H_{62}N_4O_4Cu_3 (M+2))^+$). Analysis calculated for $C_{82}H_{62}N_4O_4Cu_3 \cdot 1.5(H_2O)$: C, 71.11; H, 4.73; N, 4.05. Found: C, 71.31; H, 5.03; N, 3.94.

Cu_3 complex ((S)-5b): This compound was prepared from (S)-4b according to the procedure for (S)-5a. Yield 80%. 1H -NMR (400 MHz, δ -value, at 313K in $CDCl_3$); 11.01, 8.04, 7.78, 6.67, 5.17 (5 broad signals, 20H, 1,1'-binaphthyl-4,4',5,5',7,7',6,6',8,8'-H); 7.37 (broad signal, 2H, phenyl-p-H); 7.18 (broad signal, 4H, phenyl-m-H); 6.88 (broad signal, 4H phenyl-o-H); 10.84, 9.88, 7.90, 3.59 (4 broad signals, 16H diastereotopic pyrrole β - CH_2 Me); 1.87, 1.13 (2 broad signals, 24H, pyrrole β - CH_2 Me).

UV-vis (λ_{\max} (log ϵ) in CH_2Cl_2) 354 (4.78), 416 (sh, 3.97), 580 (sh, 4.67), 621 (4.82), 639 (sh, 4.79). FAB-MS 1412.86/1413.33 (found/calculated for $(\text{C}_{86}\text{H}_{70}\text{N}_4\text{O}_4\text{Cu}_3 (\text{M}+2))^+$). Analysis calculated for $\text{C}_{86}\text{H}_{70}\text{N}_4\text{O}_4\text{Cu}_3 \cdot 4.5(\text{H}_2\text{O})$: C, 69.08; H, 5.33; N, 3.75. Found: C, 68.88; H, 5.11; N, 3.80.

Ni₃ complex ((S)-6a): A mixture of the macrocyclic ligand ((S)-4a) (10 mg, 0.009 mmol), $\text{Ni}(\text{OAc})_2 \cdot 4\text{H}_2\text{O}$ (13.5 mg, 0.054 mmol), toluene (5 mL), MeOH (5 mL), and triethylamine (20 mg, 0.2 mmol) was refluxed for 5 h with stirring. The color of the solution turned blue. After removal of the solvent under vacuum, column chromatography on silica gel with toluene as the eluent gave a blue fraction. Recrystallization from CH_2Cl_2 -MeOH afforded 7.1 mg of the Ni₃ complex. Yield 68%. ¹H-NMR (400 MHz, δ -value, at 303 K in CDCl_3); 24.4, 10.38, 9.14, 4.87 (very broad), 3.46 (5 broad signals, 20H, 1,1'-binaphthyl aromatic protons); 7.40 (broad signal, 6H, phenyl-*o,p-H*); 7.20 (broad signal, 4H, phenyl-*m-H*); 2.40 (broad signal, 12H, pyrrole β -Me); 1.99, 1.67 (2 broad signals, 8H, diastereotopic pyrrole β -CH₂Me); 0.60 (broad signal, 12H, pyrrole β -CH₂Me). UV-vis (λ_{\max} (log ϵ) in CH_2Cl_2) 364 (4.75), 579 (4.67), 616 (4.88). ESI-MS 1342.18/1342.28 (found/calculated for $(\text{C}_{82}\text{H}_{62}\text{N}_4\text{O}_4\text{Ni}_3 (\text{M}+2))^+$). Analysis calculated for $\text{C}_{82}\text{H}_{62}\text{N}_4\text{O}_4\text{Ni}_3 \cdot 2(\text{CH}_3\text{OH}) \cdot (\text{H}_2\text{O})$: C, 70.77; H, 5.09; N, 3.93. Found: C, 70.94; H, 4.99; N, 3.84.

Ni₃ complex ((S)-6b): This compound was prepared from a macrocyclic ligand ((S)-4b) according to the procedure for (S)-6a. Yield 52%. ¹H-NMR (400 MHz, δ -value, at 293 K in CDCl_3); 24.95, 10.42, 9.12, 4.55, 3.33 (5 broad signals, 20H, 1,1'-binaphthyl aromatic protons); 7.39 (broad signal, 6H, phenyl-*o,p-H*); 7.19 (broad signal, 4H, phenyl-*m-H*); 2.78, 2.63, 1.99, 1.63 (4 broad signals, 16H, diastereotopic pyrrole β -CH₂Me); 1.23, 0.57 (2 broad signals, 24H, pyrrole β -CH₂Me). UV-vis (λ_{\max} (log ϵ) in CH_2Cl_2) 364 (4.60), 580 (4.54), 616 (4.69). Fast Atom Bombardment (FAB)-MS 1399.69/1399.35 (found/calculated for $(\text{C}_{86}\text{H}_{70}\text{N}_4\text{O}_4\text{Ni}_3 (\text{M}+2) + \text{H})^+$). Analysis calculated for $\text{C}_{86}\text{H}_{70}\text{N}_4\text{O}_4\text{Ni}_3 \cdot 1.5(\text{H}_2\text{O}) \cdot (\text{C}_6\text{H}_{14})$: C, 73.04; H, 5.80; N, 3.70. Found: C, 73.17; H, 5.99; N, 3.93.

X-ray crystallography: Diffraction data were collected using a Bruker Smart 1000 diffractometer equipped with a charge-coupled device (CCD) detector. The Sadabs program was applied for empirical absorption correction. The Shelxtl 97 program package was used for structure solution and refinement via full-matrix least-squares calculations on F^2 [40]. The hydrogen atoms were included at standard positions without refinement. Crystal data for (S)-5a recrystallized from CH_2Cl_2 -hexane: Formula $\text{C}_{82}\text{H}_{62}\text{Cu}_3\text{N}_4\text{O}_4 \cdot 6\text{H}_2\text{O}$, $M_w = 1466.08$, hexagonal, space group $P3_221$, $a = b = 22.7984(16)$, $c = 15.2704(13)$ Å, $V = 6873.7(9)$ Å³, $Z = 3$, $D_{\text{calc}} = 1.063 \text{ Mg/m}^3$, $\mu(\text{Mo-K}\alpha) = 0.739 \text{ mm}^{-1}$, $T = 299(2)$ K, final R indices [$I > 2 \sigma(I)$]: $R_1 = 0.0952$, $wR_2 = 0.2267$, $GOF = 0.952$, Some crystallographic data are summarized in Table 1. The CCDC reference number is 842598.

Magnetic susceptibility: The variable-temperature magnetic susceptibilities were measured on polycrystalline samples (5.32 mg of (S)-5a and 4.24 mg of (S)-6a) with a Quantum Design MPMS SQUID magnetometer operating in a magnetic field of 10,000 gauss at the 5 K intervals between 300 K and 50 K and at 1 K intervals between 50 K and 2 K. The diamagnetic corrections were evaluated from Pascal's constants for all the constituent atoms [41].

Theoretical calculation: Spin density was calculated using the Gaussian 09 program [42]. Initial geometry was obtained from the X-ray structure of (S)-5a, but the axial water ligand on the central Cu atom was removed. The calculation was performed both on the quartet state and on the doublet state without any symmetry restriction by using the density functional theory (DFT) method with unrestricted ωB97XD functional and B3LYP functional, employing a basis set of 6-31G(d) for C, H, N, and O and LANL2DZ for Cu.

3. Results and Discussion

3.1. Synthesis of Porphyrin Analogues

We previously reported that 2-borylpyrrole can be readily prepared and successfully used for Suzuki-Miyaura cross-coupling reactions with various aromatic bromides and iodides [38,39]. Thus, bis(pyrrol-2-yl)arenes as unique building blocks for porphyrin analogues are obtainable

from a number of commercially available aromatic dihalides. However, a standard procedure using a $\text{Pd}(\text{OAc})_2/\text{PPh}_3$ catalyst system in DMF in the presence of K_2CO_3 did not work well when 5-carboethoxy-4-ethyl-3-methyl-2-(4,4,5,5-tetramethyl-1,3,2-dioxaborolan-2-yl)pyrrole **1a** was reacted with (*S*)-3,3'-diiodo-1,1'-bi-2-naphthol [43,44]. The target cross-coupling product was obtained in moderate yield when tris(dibenzylideneacetone)dipalladium ($\text{Pd}_2(\text{dba})_3$) and tricyclohexylphosphine ($\text{P}(\text{Cy})_3$) were used according to the modified protocol for inactivated substrates [45,46]. (*S*)-3,3'-Bis(5-carboethoxy-4-ethyl-3-methylpyrrol-2-yl)-1,1'-bi-2-naphthol (*S*)-**2a** was obtained in 60% yield directly from (*S*)-3,3'-diiodo-1,1'-bi-2-naphthol (Scheme 1). (*S*)-**2a** was converted into (*S*)-3,3'-bis(4-ethyl-3-methylpyrrol-2-yl)-1,1'-bi-2-naphthol (*S*)-**3a** in 83% yield via a hydrolysis–decarboxylation sequence. The traditional Rothmund-type condensation of (*S*)-**3a** and benzaldehyde was done in the presence of a catalytic amount of TFA. Subsequent DDQ oxidation afforded 58% yield of the binaphthol-embedded porphyrin analogue (*S*)-**4a** [47]. The $^1\text{H-NMR}$ spectrum of (*S*)-**4a** shows a pair of multiplets due to the diastereotopic methylene protons of the pyrrole- β -ethyl group at $\delta = 1.87$ and 1.65 ppm. These protons are in the magnetically anisotropic environment and shifted to a lower-frequency region in comparison with the corresponding protons of (*S*)-**3a** that appear at $\delta = 2.55$ ppm as a single quartet (Supplementary Materials, Figures S2 and S3). This is because of the restricted conformational freedom of the ethyl group and the ring current effect of the *meso*-like phenyl group of (*S*)-**4a** on the neighboring methylene protons. The 5-, 6-, 7-, and 8-naphthyl protons of (*S*)-**4a** at $\delta = 7.80$, 7.24, 7.16, and 7.00 ppm are shifted by 0.10–0.15 ppm to the lower-frequency regions compared to those of (*S*)-**3a**, but the 4-naphthyl proton at $\delta = 8.34$ ppm appeared at a higher frequency by 0.24 ppm. The observed mass at 1173.40 by ESI-TOF-MS is in accordance with the theory (1173.53 for $(\text{M} + \text{H})^+$) of (*S*)-**4a**. Homologs, (*S*)-**2b**, (*S*)-**3b**, and (*S*)-**4b**, were similarly synthesized from 5-carboethoxy-3,4-diethyl-2-(4,4,5,5-tetramethyl-1,3,2-dioxaborolan-2-yl)pyrrole **1b**. It was also confirmed via HPLC analysis on a chiral phase that the synthetic transformations from (*S*)- and (*R*)-3,3'-diiodo-1,1'-bi-2-naphthol to (*S*)-**4a** and (*R*)-**4a**, respectively, did not reduce the original optical purity (Figure S10, Supplementary Materials). The CD spectrum of (*S*)-**4a** in CH_2Cl_2 shows a positive first Cotton effect and a negative second Cotton effect at 591 nm and 530 nm, respectively. A mirror image CD couplet was observed for (*R*)-**4a** (Figure 2 and Figure S10, Supplementary Materials).

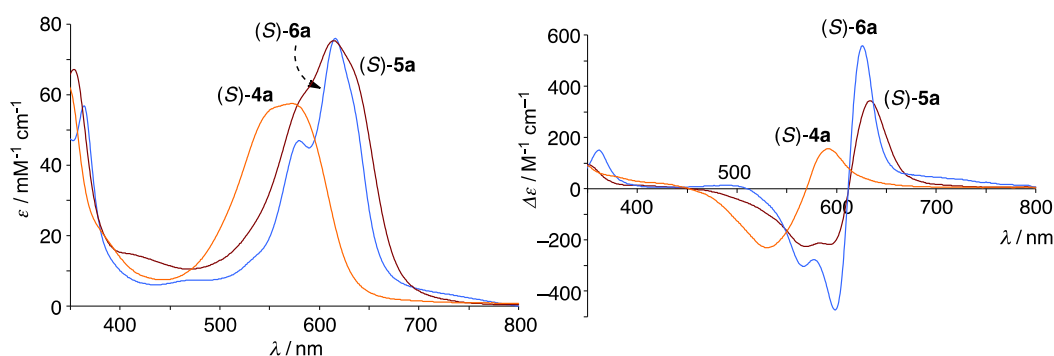


Figure 2. Ultraviolet (UV)–vis (left) and circular dichroism (CD) (right) spectra of (*S*)-**4a** (orange line), (*S*)-**5a** (brown line), and (*S*)-**6a** (blue line) in CH_2Cl_2 .

Metalation of (*S*)-**4a** with $\text{Cu}(\text{OAc})_2 \cdot 2\text{H}_2\text{O}$ in CH_2Cl_2 –MeOH containing triethylamine at room temperature for 5 h afforded the trinuclear copper complex (*S*)-**5a** in 67% yield. The observed mass of (*S*)-**5a** at 1357.08 by ESI-TOF-MS is in accordance with the theory (1357.28 for $(\text{M} + 2)^+$) of the Cu^{II}_3 complex of the hexaanionic (*S*)-**4a** with no additional ligand. The UV–vis absorption band of (*S*)-**5a** appeared at 614 nm. This is red-shifted by 42 nm with respect to the 572 nm band of (*S*)-**4a**. (*S*)-**5a** showed a positive CD couplet at 634 nm as a first Cotton effect and split negative peaks at 593 and 569 nm. The trinuclear nickel complex (*S*)-**6a** was prepared in 68% yield by refluxing a toluene–MeOH solution of (*S*)-**4a**, $\text{Ni}(\text{OAc})_2 \cdot 4\text{H}_2\text{O}$, and triethylamine for 5 h. The observed mass of (*S*)-**6a** at 1342.18 by

ESI-TOF-MS is in accordance with the theory (1342.28 for $(M + 2)^+$) of the Ni^{II}_3 complex of hexaanionic (*S*)-**4a** with no additional ligand. (*S*)-**6a** shows a UV-vis absorption band at 616 nm and a CD first Cotton effect at 626 nm with split negative peaks at 598 and 567 nm (Figure 2).

3.2. Structure of Trinuclear Complexes

X-ray crystallography of (*S*)-**5a** shows three linearly aligned Cu atoms where the central Cu atom is shared between two Cu_2O_2 diamond cores (Figure 3) [17]. The $Cu(1)-Cu(2)-Cu(1')$ angle is 174.7° and two Cu_2O_2 mean planes make a small plane-to-plane angle of 8.3° . Deviation of each atom of Cu_2O_2 from the Cu_2O_2 mean plane is less than 0.012 \AA , which indicates that the Cu_2O_2 diamond core of (*S*)-**5a** is quite planar compared with previously reported tricopper complexes [18–24,48–51]. These structural features allow a strong metal–metal coupling. The terminal Cu atoms are in a distorted square planar coordination environment composed of dipyrin nitrogens and binaphthol oxygens, where the $N(1)-Cu(1)-N(2)$ plane and the $O(1)-Cu(1)-O(2)$ plane are twisted by 30.7° . The central Cu atom in a square pyramidal coordination environment is ligated by four binaphthol oxygens as a basal plane and water oxygen weakly in an apical position. The $Cu(2)$ atom is deviated by 0.093 \AA from the mean basal plane toward the apical ligand, and the $Cu(2)-O(3)$ distance (2.43 \AA) is much longer than the $Cu(2)-O(2)$ and $Cu(2)-O(1)$ distances (1.922 and 1.949 \AA).

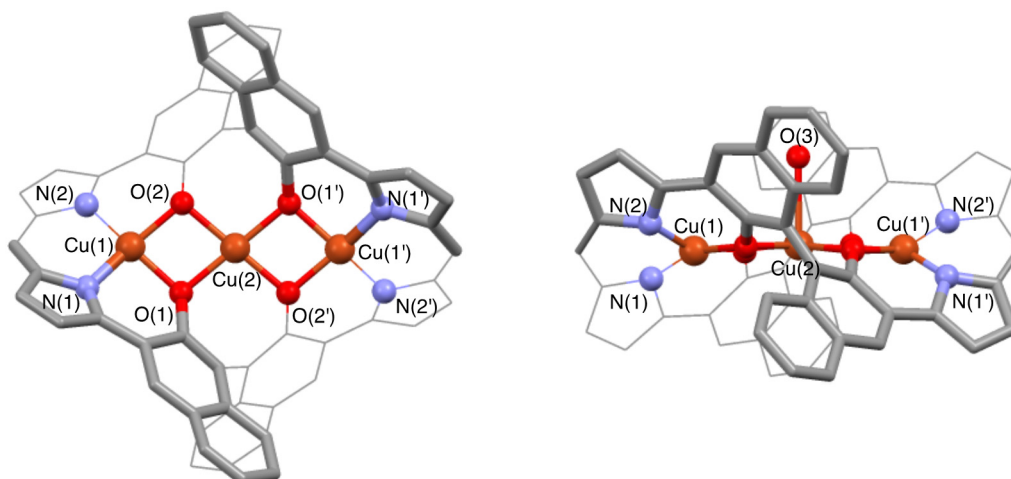


Figure 3. X-ray diagrams of (*S*)-**5a** with peripheral alkyl groups and phenyl groups omitted for clarity (reproduced from the preliminary communication [17]). A bottom view (**left**) and a front view (**right**) with atom numbering scheme.

A number of multidentate ligands (L) of a N_2O_2 donor set are known to form trinuclear complexes, where three metals are assembled by μ -alkoxy bridges (Figure 4) [48–53]. This Cu_3O_4 core is planar or folded depending on the N_2O_2 ligand structure and the apical site coordination. X-ray data of such $(L)M(\mu-OR)_2M(\mu-OR)_2M(L)$ complexes are shown in Table 1. The Cu_3O_4 core of **7** and **9** having four-coordinated Cu^{II} ions at both terminal sites is rather unusual [52,53]. (*S*)-**5a** is similar to **7** in this sense, but the $Cu(1)-Cu(2)$ distance (2.910 \AA) of (*S*)-**5a** is the shortest among these linear tricopper complexes. Although the basal plane of the central Cu^{II} ion of **7** is completely planar, the Cu_2O_2 unit of **7** is less planar than that of (*S*)-**5a**, as seen in the deviation (0.060 \AA for **7** and 0.012 \AA for (*S*)-**5a**) of each atom of Cu_2O_2 from the Cu_2O_2 mean plane [52]. Two $Cu(\text{salen})$ units are in a crossing arrangement in the tricopper complex **9**, as well as two dipyrin units of (*S*)-**5a**, as seen in the side view of Figure 3 [53]. This structural feature leads to the highly distorted square planar geometry of the terminal Cu^{II} ions of (*S*)-**5a** and the trigonal bipyramid geometry of the central Cu^{II} ion in the complex **9**. As a result, the $Cu(1)-Cu(2)-Cu(1')$ angle of **9** is 156.2° and the $Cu(2)-OH_2$ distance of **9** (2.177 \AA) is shorter than that (2.43 \AA) of (*S*)-**5a**. The tricopper complex **10** is a rare example having the Cu_3O_4 unit inside the macrocycle [31], but its intrinsically folded ligand structure causes the $Cu(1)-Cu(2)-Cu(1')$ angle of

127.8°. X-ray crystallographic studies on the trinuclear complexes of the Ni₃O₄ core indicated that Ni^{II} ions are usually six-coordinated [25–30,54–58]. The complex **8** is a rare example where only the central Ni is six-coordinated [52]. Although we could not get X-ray data of the Ni₃ complex (S)-**6a**, very similar UV–vis and CD spectra of (S)-**5a** and (S)-**6a** point to their structural similarity. It is considered on the basis of the X-ray structure of (S)-**5a** that the terminal Ni^{II} ions of (S)-**6a** are four-coordinated and the central Ni ion is six-coordinated like **8** (vide infra). Coordination of external ligands to the central Ni ion of (S)-**6a** is suggested by elemental analysis.

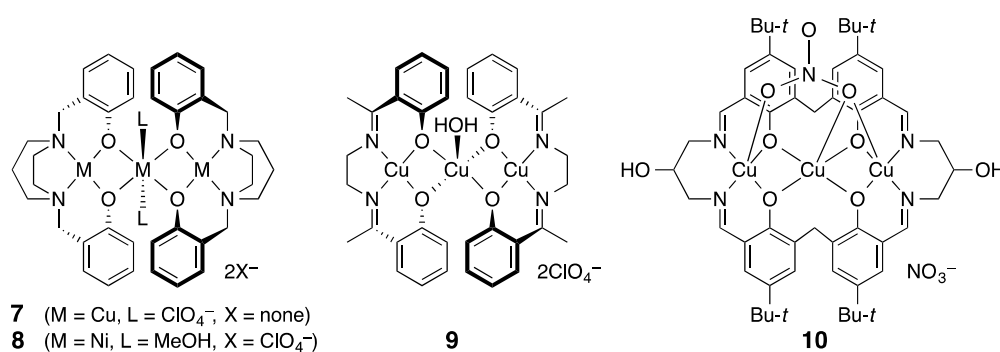


Figure 4. Trinuclear Cu and Ni complexes of tetradentate ligands of a N₂O₂ donor set.

Table 1. X-ray structural data (distance (Å) and angle (°)) of the Cu₃O₄ core of (S)-**5a**, **7**, **8**, **9**, and **10**¹.

	(S)- 5a	7	8	9	10
M(1)–O(1)	1.877	1.927	1.873	1.877–1.899	1.945–1.957
M(1)–O(2)	1.893	1.929			
M(2)–O(1)	1.949	1.953	2.041	1.930, 1.949	1.918–1.929
M(2)–O(2)	1.922	1.956	2.050	1.977, 2.065	
M(2)–O(apical)	2.43	2.589	2.067	2.177	2.491
M(1)–M(2)	2.910	2.938	3.007	2.950, 2.975	2.843, 2.861
M(1)–O(1)–M(2)	98.5	98.3	100.0	97.6–101.6	94.1–95.3
M(1)–O(2)–M(2)	100.0	98.4	100.4		
O(1)–M(1)–O(2)	82.1	80.5	83.8	76.8, 76.7	77.5–81.4
O(1)–M(2)–O(2)	79.5	81.9	75.4		
M(1)–M(2)–M(1')	174.7	180	180	156.2	127.8

¹ Taken from [17,31,52,53]. M(1) and M(2) denote terminal and central metal, respectively. O(1) and O(2) denote phenolic oxygen.

3.3. ¹H-NMR Spectra of Paramagnetic Trinuclear Complexes

The presence of three *d*⁹ Cu^{II} ions in (S)-**5a** leads to paramagnetism. The magnetic moment (3.2 B.M.) of (S)-**5a** was measured by the Evans method in CDCl₃ at 293 K. That is close to the spin-only theoretical value (3.0 B.M.) for the molecular system of three noninteracting S = 1/2 electron spins [59–61]. It is noteworthy that all the ¹H-NMR signals of (S)-**5a** are observed owing to the fast electron spin relaxation. Two signals of a 12H-integral at δ = 0.98 and 7.11 ppm at 303 K in CDCl₃ are assigned to the methyl protons of the pyrrole β-ethyl and β-methyl group, respectively (Figure 5, top and Figure S4, Supplementary Materials). The 2D-COSY experiment indicated that two signals of a 4H-integral at δ = 9.61 and 3.28 ppm are associated with the methylene protons of the ethyl group (Figure S8). Correlation was also observed for three signals at δ = 7.38 (2H), 7.20 (4H), and 6.88 ppm (4H) assigned to the *meso*-phenyl protons. The naphthyl protons are associated with the remaining five signals of a 4H-integral at δ = 10.79, 7.99, 7.72, 6.80, and 5.25 ppm. Relatively sharp signals at 7.99, 7.72, and 6.80 ppm should be assigned to the 5-, 6-, and 7-naphthyl protons, and broad signals at δ = 10.79 and 5.25 ppm must be due to the 4- and 8-naphthyl protons that are closer to the metal centers (Table S1, Supplementary Materials). Since the four signals are correlated by the COSY cross-peaks that revealed their positional sequence ((7.99)↔(6.80)↔(7.72)↔(5.25)), they are assigned to the 5-, 6-,

7-, and 8-naphthyl protons, respectively (see Scheme 2 for atom numbering). Consequently, the signal at 10.79 ppm with no correlation is assigned to the 4-naphthyl proton.

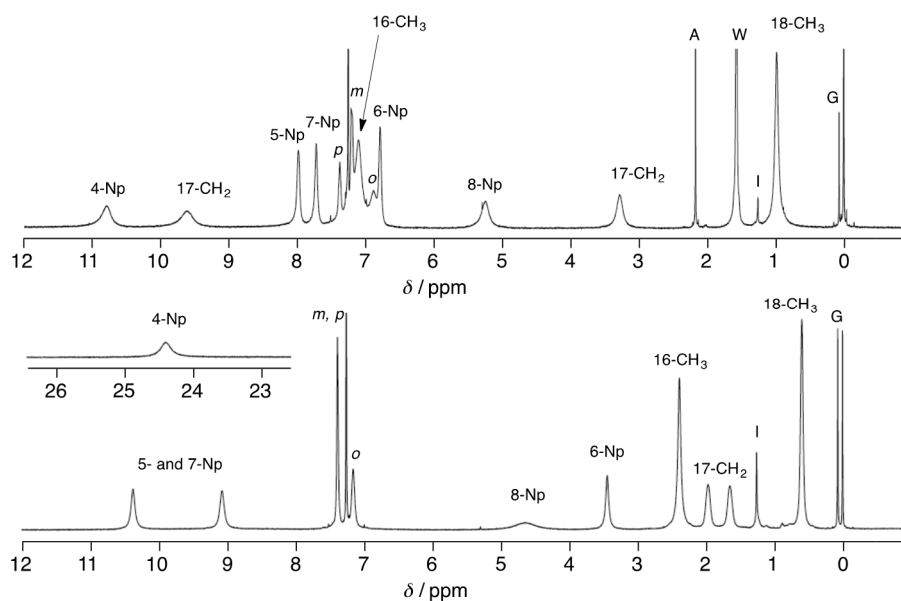
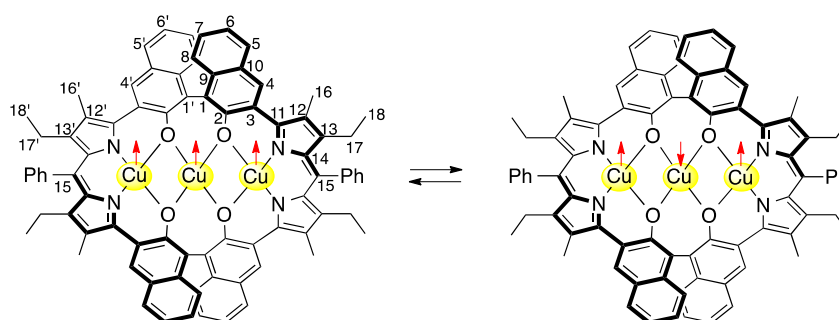


Figure 5. $^1\text{H-NMR}$ spectra of (*S*)-**5a** (top) and (*S*)-**6a** (bottom) in CDCl_3 at 303 K. Naphthyl (Np), *meso*-phenyl (*o*, *m*, *p*), methylene (CH_2), and methyl (CH_3) protons are labeled. Signals due to water (W), acetone (A), grease (G), and impurity (I) are seen. See Scheme 2 for atom numbering.



Scheme 2. Spin-state equilibrium of (*S*)-**5a**.

Theoretical DFT calculation (6-31G(d), LANL2DZ/ ω B97XD) of the spin density for the quartet spin state of (*S*)-**5a** on the basis of the X-ray structure indicates that a positive spin appears at the pyrrole β -carbons (C12, C13) and at the naphthyl 6- and 8-carbons, while a negative spin appears at the naphthyl 4-, 5- and 7-carbons (Table 2 and Table S3, Supplementary Materials). It is considered that a negative electron spin at the naphthyl 4-, 5- and 7-carbons induces positive spin polarization at the naphthyl 4-, 5- and 7-protons by way of spin exchange mechanism, while a positive spin at the pyrrole β -carbons (C12, C13) also induces positive spin polarization at the directly attached 16- CH_3 and 17- CH_2 protons by way of hyperconjugation mechanism [62,63]. This positive spin polarization at the 4-, 5-, and 7-naphthyl protons and the 16- CH_3 and 17- CH_2 protons is expected to cause a high-frequency shift of their paramagnetic $^1\text{H-NMR}$ signals with respect to their normal diamagnetic chemical shifts; on the other hand, a positive spin at the 6- and 8-naphthyl carbons results in a low-frequency shift for the 6- and 8-naphthyl protons. The observed $^1\text{H-NMR}$ chemical shifts of (*S*)-**5a** at 303 K are consistent with the DFT-based paramagnetic $^1\text{H-NMR}$ shifts under the assumption that the paramagnetic shift depends primarily on the contact shift that is directly related to the spin density in the $S = 3/2$ spin state.

Table 2. Spin density of (S)-5a calculated by DFT (6-31G(d), LANL2DZ/ ω B97XD)¹.

	S = 1/2		S = 3/2	
Cu(1), Cu(1')	0.5977		0.6083	
Cu(2)	−0.6169		0.6366	
naphthyl-O(1),O(1')	−0.0018	−0.0032	0.1428	0.1453
dipyrroin-N(1),N(1')	0.1061	0.1051	0.1099	0.1093
naphthyl-C(4),C(4')	0.0061	0.0069	−0.0082	−0.0092
naphthyl-C(5),C(5')	0.0047	0.0053	−0.0052	−0.0058
naphthyl-C(6),C(6')	−0.0060	−0.0067	0.0066	0.0073
naphthyl-C(7),C(7')	0.0043	0.0048	−0.0048	−0.0053
naphthyl-C(8),C(8')	−0.0054	−0.0060	0.0063	0.0070
pyrrole β -C(12),C(12')	0.0034	0.0036	0.0047	0.0053
pyrrole β -C(13),C(13')	0.0072	0.0072	0.0067	0.0062
methyl-C(16),C(16')	0.0010	0.0010	0.0009	0.0009
methylene-C(17),C(17')	0.0004	0.0003	0.0005	0.0004

¹ See Scheme 2 for atom numbering.

Since the ¹H-NMR spectral pattern of (S)-5a is consistent with a D₂ symmetric structure, the apical water ligand observed in the X-ray structure seems to dissociate in solution. Plotting the ¹H-NMR chemical shifts against T^{−1} on the basis of the variable-temperature (VT) ¹H-NMR data of (S)-5a showed linear correlation, and the chemical shift extrapolated to the point of T^{−1} = 0 for each proton signal is shown at the left end of the least square approximation line in Figure 6a (Figure S4, Supplementary Materials). Replacement of the pyrrole- β 16-CH₃ group of (S)-5a by the ethyl group in the case of (S)-5b did not affect the position and the temperature dependency of the ¹H-NMR signals due to the naphthyl protons (red circle in Figure 6a,b) and meso-phenyl protons (black triangle in Figure 6a,b) at all. However, signals due to the 17-CH₂ protons at the pyrrole β -position next to the meso-phenyl group slightly shifted from δ = 9.1 and 3.4 ppm for (S)-5a to δ = 10.6 (or 9.7) and 3.7 ppm for (S)-5b at 323 K, while the signals due to the pyrrole β -16-CH₃ protons at δ = 7.0 ppm (filled blue square in Figure 6a) of (S)-5a were replaced by the newly introduced ethyl protons of (S)-5b that appeared at δ = 9.7 (or 10.6) and 7.8 (CH₂), and 1.9 (CH₃) ppm at 323 K (Figure 6b and Figure S5, Supplementary Materials). Signals due to the naphthyl 6- and 8-protons of (S)-5a and (S)-5b move to the lower-frequency region with increasing temperature, while the signal due to the 4-naphthyl proton moves to the higher-frequency region with increasing temperature. The chemical shifts extrapolated to the point of T^{−1} = 0 are far from normal diamagnetic chemical shift region of the naphthyl 4-, 6-, and 8-protons in contrast to the relatively normal Curie law profile of the signals due to the pyrrole β -methyl and β -methylene protons of (S)-5a and (S)-5b. This Curie plot profile of (S)-5a and (S)-5b is explained in terms of the temperature-dependent equilibrium of spin states. DFT calculation indicates that the spin density at the central Cu ion has the opposite sign between the quartet spin state (0.64) and the doublet spin state (−0.62) (Table 2). However, the spin densities at the terminal Cu ions have the same sign for the quartet (0.61) and the doublet (0.60). Accordingly, the spin densities at the pyrrole β -carbons (C12, C13) that are transmitted from the terminal Cu ions have the same sign (positive) for both spin states, but the spin densities at the naphthyl carbons that are transmitted strongly from the central Cu ion show opposite sign for these two spin states. The DFT calculation indicates that the doublet spin state is expected to cause a low-frequency shift for the ¹H-NMR signals of the 4-, 5-, and 7-naphthyl protons and a high-frequency shift for the 6- and 8-naphthyl protons in contrast to the quartet spin state. The observed Curie plot profile of (S)-5a and (S)-5b at low temperatures seems consistent with that expected for the doublet spin state.

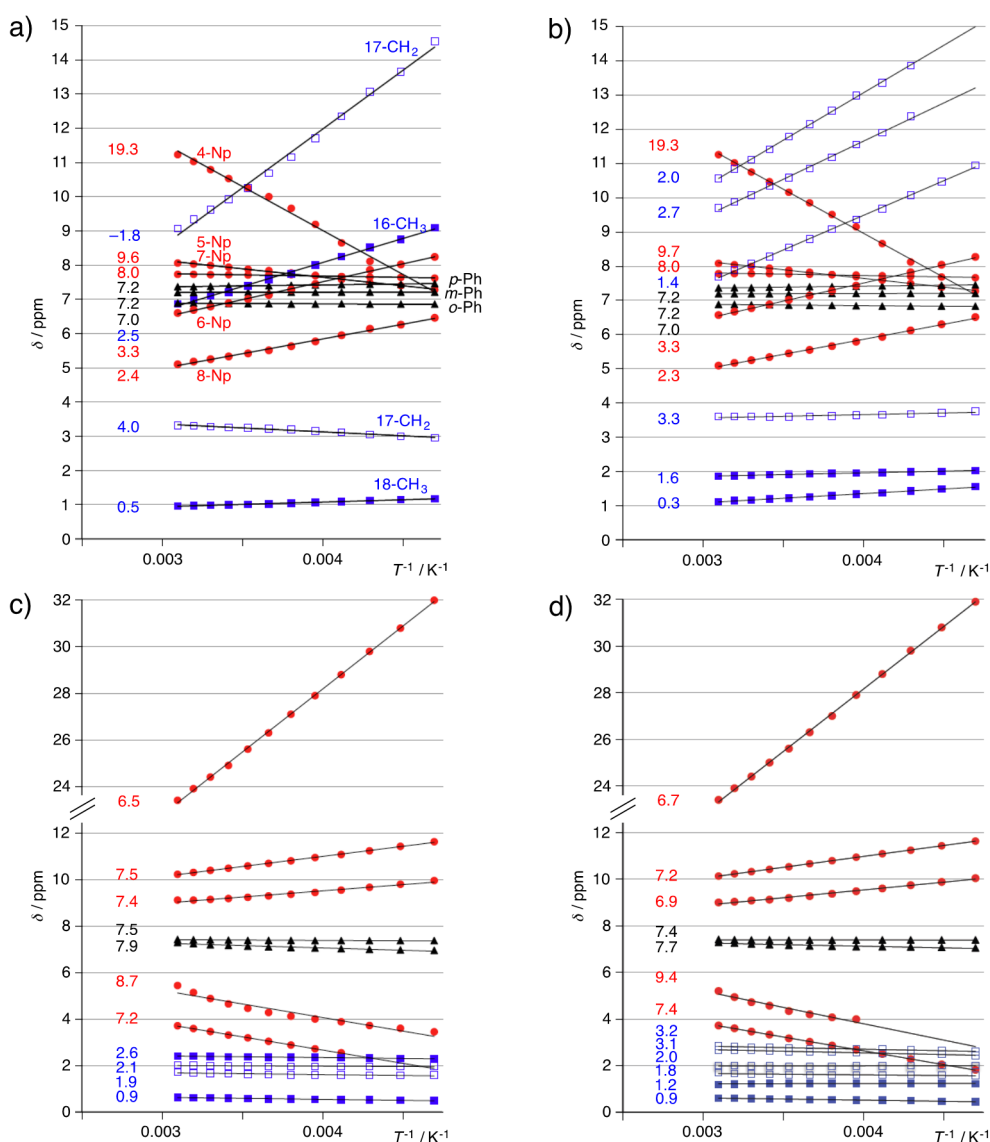


Figure 6. Plots of the $^1\text{H-NMR}$ chemical shifts (δ) of (a) (S)-5a, (b) (S)-5b, (c) (S)-6a, and (d) (S)-6b in CDCl_3 against T^{-1} (K^{-1}) (10° interval from 323 K to 213 K). CH_3 protons (filled blue square); CH_2 protons (blue square); *meso*-phenyl protons (black triangle); naphthyl protons (red circle). The δ -values extrapolated to $T^{-1} = 0$ in the linear approximation of a series of the observed data are shown at the left end of each line. See Scheme 2 for atom numbering.

DFT calculation of (S)-5a in the doublet state using the B3LYP functional showed the nonsymmetric Cu_3O_4 core in contrast to the symmetric Cu_3O_4 core obtained by using the ωB97XD functional (Figure S13 and Table S2, Supplementary Materials), i.e., two Cu(terminal)–Cu(center) distances (2.887 Å and 3.055 Å) in the B3LYP case and a single Cu–Cu distance (2.930 Å) in the ωB97XD case. The calculated spin densities of the Cu^{II}_3 unit in the B3LYP case are Cu(0.5588)–Cu(0.0067)–Cu(−0.0007) in sequence (Table S4, Supplementary Materials). This is quite different from the symmetric spin structure (Cu(0.5977)–Cu(−0.6169)–Cu(0.5977)) of the ωB97XD case. As for the quartet state of (S)-5a, both DFT calculations using the B3LYP and ωB97XD functional resulted in a symmetric Cu_3O_4 core with a Cu–Cu distance of 2.922 Å and 2.911 Å, respectively, and their calculated spin densities of the Cu^{II}_3 unit are Cu(0.5644)–Cu(0.5190)–Cu(0.5654) in sequence for the B3LYP case and Cu(0.6083)–Cu(0.6366)–Cu(0.6083) in sequence for the ωB97XD case (Figure S13, Tables S2 and S4, Supplementary Materials). The observed $^1\text{H-NMR}$ paramagnetic shifts for the naphthyl protons of

(*S*)-**5a** at both limits of high and low temperature are correlated with the calculated spin densities at the naphthyl unit in the $S = 3/2$ and $1/2$ spin state, respectively. This correlation with the spin densities using the ω B97XD functional is much better than those using the B3LYP functional (Table 2 and Table S4, Supplementary Materials).

The magnetic moment (4.6 B.M.) of (*S*)-**6a** was measured using the Evans method in CDCl_3 at 293 K. This is close to the spin only theoretical value (4.9 B.M.) for the molecular system of three noninteracting d^8 ($S = 1$) Ni^{II} ions. The $^1\text{H-NMR}$ spectrum of (*S*)-**6a** at 303 K in CDCl_3 shows two 12H-signals at $\delta = 0.61$ and 2.39 ppm due to the methyl protons of the pyrrole β -ethyl and β -methyl group, respectively (Figure 5, bottom). The 2D-COSY experiment reveals that two 4H-signals at $\delta = 1.99$ and 1.67 ppm are associated with the diastereotopic methylene protons of the pyrrole β -ethyl group (Figure S9, Supplementary Materials). The 6H-signal at 7.40 ppm and the 4H-signal at 7.20 ppm are also assignable to the *meso*-phenyl protons. The remaining five 4H-signals at $\delta = 24.4$, 10.38, 9.14, 4.87 (very broad), and 3.46 ppm are associated with the naphthyl protons. Three relatively sharp signals are associated with 5-, 6-, and 7-naphthyl protons that showed 2D-COSY cross-peaks of the signal at $\delta = 3.46$ ppm against signals at $\delta = 9.14$ and 10.83 ppm. Consequently, the signal at $\delta = 3.46$ ppm is associated with the 6-naphthyl proton, and the signals at $\delta = 9.14$ and 10.83 ppm are associated with the 5- and 7-naphthyl protons. These remarkable paramagnetic shifts in the opposite direction for the closely positioned 5-, 6-, and 7-naphthyl protons are ascribable not to the dipolar term but to the contact term. The directions of these paramagnetic shifts of the 5-, 6-, and 7-naphthyl protons of (*S*)-**6a** are similar to those of (*S*)-**5a** at 303 K. Therefore, the high-frequency-shifted signal at 24.4 ppm and the low-frequency-shifted signal at 4.87 seem to be associated with the 4- and 8-naphthyl protons, respectively. These remarkable chemical shifts and the temperature dependency of the naphthyl protons are not affected by replacing the pyrrole β -methyl group of (*S*)-**6a** by the ethyl group in the case of (*S*)-**6b** (Figure 6c,d, and Figures S6 and S7, Supplementary Materials). Since the Curie plots of (*S*)-**6a** and (*S*)-**6b** show that the chemical shifts extrapolated to the point of $T^{-1} = 0$ for all the proton signals are in their normal diamagnetic chemical shift range, the spin state is not greatly affected by temperature change, and the magnetic coupling between nickel ions should be not so important as the case of the copper ions. The proton signals due to the dipyrin part of (*S*)-**6a** and (*S*)-**6b** are in the normal diamagnetic chemical shift range, and their temperature dependency is negligible (blue squares in Figure 6a,b). Therefore, the dipolar term of the paramagnetic shift should be negligible in the dipyrin part not only of (*S*)-**6a** and (*S*)-**6b** but also of (*S*)-**5a** and (*S*)-**5b**. It is noteworthy that the spin density is not transferred from the terminal nickel ion to the pyrrole ligand, but the partial spin is transferred to the 1,1'-binaphthol ligand.

The Curie plot of the trinuclear Cu^{II} complexes does not show a normal Curie law profile. The chemical shifts of the 4-, 6-, and 8-naphthyl proton of (*S*)-**5a** and (*S*)-**5b** move further away from the normal diamagnetic chemical shift range as temperature goes up from 213 K to 323 K, and they are extrapolated to 19.3, 3.3, and 2.3 ppm, respectively, at $T^{-1} = 0$ (Figure 6a). This suggests that the magnetic moment of the trinuclear Cu^{II} complexes increases as temperature goes up as a result of decreasing antiferromagnetic coupling interaction. While the chemical shifts of the pyrrole β -methyl and β -ethyl protons of (*S*)-**6a** and (*S*)-**6b** are not affected at all by the paramagnetism even though those signals are broadened, the corresponding protons of (*S*)-**5a** and (*S*)-**5b** undergo remarkable paramagnetic shifts. Accordingly, these paramagnetic shifts of (*S*)-**5a** and (*S*)-**5b** are caused by the contact term that was induced by the electron spin density on the pyrrole β -carbons through π -conjugation. Since the paramagnetic shifts observed for the pyrrole β -methyl and β -methylene protons of (*S*)-**5a** and (*S*)-**5b** are caused by the partial spin density transferred from the single terminal Cu atom where the spin state does not depend on temperature, their temperature dependency seems to show an ordinary Curie law profile. In fact, these signals are extrapolated to -1.8 , 2.5, 4.0, and 0.5 ppm for (*S*)-**5a** and 2.0, 2.7, 1.4, 3.3, 1.6, and 0.3 ppm for (*S*)-**5b**. On the other hand, the spin density of the 1,1'-binaphthol ligand is derived both from the terminal Cu atom and from the central Cu atom, and their antiparallel spin orientation would be enhanced more at lower temperature due to the antiferromagnetic coupling (Scheme 2).

A pair of Cu atoms with opposite spin causes a counterbalancing effect on the paramagnetic shifts of the binaphthol ligand. Thus, the unusual temperature dependency of the paramagnetic shifts for the binaphthol protons is ascribed to the spin equilibrium between the quartet and doublet.

3.4. Magnetic Susceptibility of Trinuclear Complexes

Magnetic susceptibility (χ_M) of the polycrystalline sample of (S)-**5a** was measured in the temperature range of 2–300 K, and the temperature dependence plot ($\chi_M T$ vs. T) is shown in Figure 7 after correction for the diamagnetic terms. The $\chi_M T$ value of $0.72 \text{ cm}^3 \cdot \text{mol}^{-1} \cdot \text{K}$ at 300 K is lower than the $1.125 \text{ cm}^3 \cdot \text{mol}^{-1} \cdot \text{K}$ expected for three noninteracting Cu^{II} ions. As temperature goes down, $\chi_M T$ decreases monotonously to reach the value of $0.375 \text{ cm}^3 \cdot \text{mol}^{-1} \cdot \text{K}$ at 15 K, which corresponds to an $S = 1/2$ ground state for $g = 2$. This behavior indicates an antiferromagnetic coupling in the Cu^{II}_3 core. A further decrease in $\chi_M T$ below this temperature to 2 K can be attributed to intermolecular interactions between $S = 1/2$ trinuclear units. Curve fitting for the temperature-dependent susceptibility data was introduced by an expression for a linear trinuclear Cu^{II} complex on the basis of the spin Hamiltonian $H = -J(S_1 S_2 + S_2 S_3)$. The theoretical equation for χ_M can be expressed by Equation (1), where θ reflects intermolecular interaction at very low temperature, and TIP stands for a temperature-independent paramagnetism [48,64]. A good data fit was obtained for $g = 1.970$, $\theta = -0.11 \text{ K}$, $J = -434 \text{ cm}^{-1}$, and $\text{TIP} = 887 \times 10^{-6} \text{ cm}^3 \text{ mol}^{-1}$, with the agreement factor R defined as $\sum_i [(\chi_M T)_{\text{obs}} - (\chi_M T)_{\text{calc}}]^2 / \sum_i [(\chi_M T)_{\text{obs}}]^2$ is 5.25×10^{-5} .

$$\chi_M = (A/B) N_A g^2 \beta^2 / 4k_B (T - \theta) + \text{TIP}, [A = 1 + \exp(J/kT) + 10 \exp(3J/2kT), \quad (1)$$

$$B = 1 + \exp(J/kT) + 2 \exp(3J/2kT)].$$

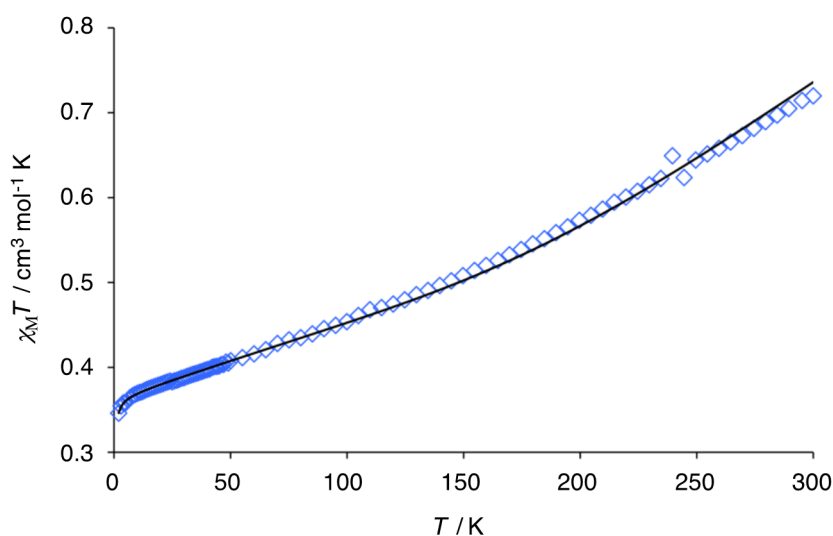


Figure 7. A plot of $\chi_M T$ vs. T of (S)-**5a**. A solid line represents a theoretical curve for the parameters $g = 1.97$, $\theta = -0.11$, $J = -434 \text{ cm}^{-1}$, and temperature-independent paramagnetism (TIP) = $887 \times 10^{-6} \text{ cm}^3 \text{ mol}^{-1}$.

It is well known that the exchange parameter J is linearly related to the Cu–O–Cu angle in the dinuclear complexes $(\text{L})\text{Cu}^{\text{II}}(\mu\text{-OR})_2\text{Cu}^{\text{II}}(\text{L})$ [65]. The J value (-434 cm^{-1}) of (S)-**5a** is in the range ($-511, -482.5, -474, -345.5 \text{ cm}^{-1}$) [48–51] reported for the μ -phenoxy-bridged linear trinuclear Cu^{II} complexes having the Cu–O–Cu angle of 101.4° – 98.3° including 7 (-314 cm^{-1}) [52]. On the other hand, a much weaker J value (-190 cm^{-1}) was reported for the bent Cu^{II}_3 complex **9** [53]. It is noteworthy that the antiferromagnetic coupling of (S)-**5a** is much stronger than the reported dinuclear ($J = -87.6 \text{ cm}^{-1}$) [2b] and trinuclear ($J = -44.1 \text{ cm}^{-1}$) [12] Cu^{II} complexes of porphyrin analogues.

A similar temperature dependence plot ($\chi_M T$ vs. T) of (S)-6a is shown in Figure 8. The $\chi_M T$ value of $2.50 \text{ cm}^3 \cdot \text{mol}^{-1} \cdot \text{K}$ at 300 K is lower than the $3.00 \text{ cm}^3 \cdot \text{mol}^{-1} \cdot \text{K}$ expected for three noninteracting high-spin ($S = 1$) Ni^{II} ions. As temperature goes down, $\chi_M T$ decreases monotonously to reach the value of $1.00 \text{ cm}^3 \cdot \text{mol}^{-1} \cdot \text{K}$ at 14 K, which corresponds to the $S = 1$ ground state for $g = 2$ per Ni^{II}_3 . This magnetic behavior clearly indicates antiferromagnetic coupling in the Ni^{II}_3 core. A further decrease in $\chi_M T$ below this temperature to 2 K is ascribable to intermolecular interactions between $S = 1$ trinuclear units. The theoretical equation for χ_M on the basis of the spin Hamiltonian $H = -2J_1(S_1S_2 + S_2S_3) - 2J_2(S_1S_3)$ ($S_1 = S_2 = S_3 = 1$) for a trinuclear nickel(II) complex is expressed by Equation (2), where J_1 and J_2 are exchange parameters between the adjacent two Ni^{II} ions and between the terminal two Ni^{II} ions, respectively [54]. The best fit was obtained at $g = 2.20$, $\theta = -2.84 \text{ K}$, $J_1 = -49 \text{ cm}^{-1}$, $J_2 = 17 \text{ cm}^{-1}$, and $\text{TIP} = 800 \times 10^{-6} \text{ cm}^3 \text{ mol}^{-1}$, with the R factor of 1.68×10^{-4} . If the magnetic interaction between the terminal Ni ions is neglected ($J_2 = 0 \text{ cm}^{-1}$), the best fit parameters are $g = 2.17$, $\theta = -2.72 \text{ K}$, $J_1 = -60 \text{ cm}^{-1}$, $\text{TIP} = 2200 \times 10^{-6} \text{ cm}^3 \text{ mol}^{-1}$, and $R = 1.60 \times 10^{-4}$.

$$\begin{aligned} \chi_M = & (A/B)N_A g^2 \beta^2 / k_B(T-\theta) + \text{TIP} \left(A = 28 \exp [2(2J_1/kT + J_2/kT)] \right. \\ & + 10 \exp [2(J_2/kT - J_1/kT)] + 10 \exp [2(J_1/kT - J_2/kT)] \\ & + 2 \exp [2(J_2/kT - 3J_1/kT)] + 2 \exp [-2(J_1/kT + J_2/kT)] \\ & + 2 \exp (-4J_2/kT), B = 7 \exp [2(2J_1/kT + J_2/kT)] \\ & + 5 \exp [2(J_2/kT - J_1/kT)] + 5 \exp [2(J_1/kT - J_2/kT)] \\ & + 3 \exp [2(J_2/kT - 3J_1/kT)] + 3 \exp [-2(J_1/kT + J_2/kT)] \\ & \left. + 3 \exp (-4J_2/kT) + \exp [-2(2J_1/kT + J_2/kT)] \right). \end{aligned} \quad (2)$$

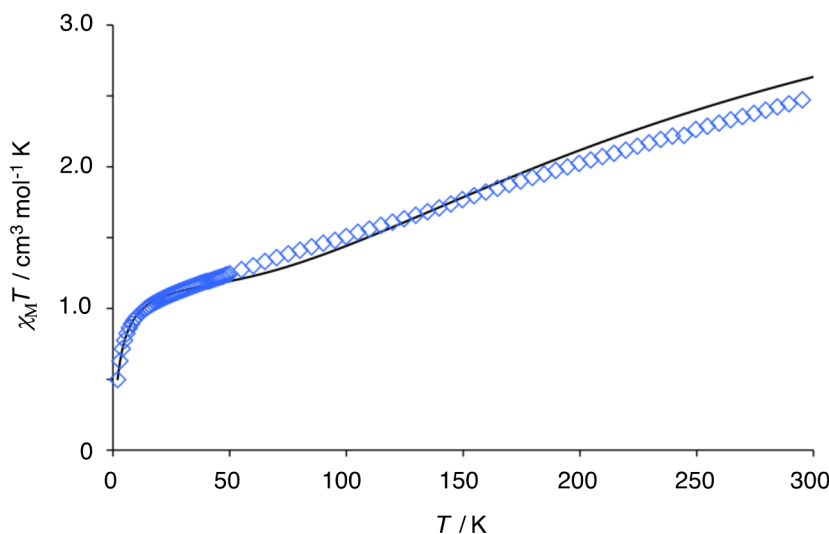


Figure 8. A plot of $\chi_M T$ vs. T of (S)-6a. A solid line represents a theoretical curve for the parameters $g = 2.20$, $\theta = -2.84$, $J_1 = -49 \text{ cm}^{-1}$, $J_2 = 17 \text{ cm}^{-1}$, and $\text{TIP} = 800 \times 10^{-6} \text{ cm}^3 \text{ mol}^{-1}$.

Studies on the magnetic properties of dinuclear Ni^{II} complexes having μ -phenoxy bridging ligands have shown that the exchange parameter J is dependent not only on the Ni–O–Ni angles but also on the coordination geometry of Ni ions [66]. That is, an antiferromagnetic exchange gets stronger as a tetragonal distortion from octahedral geometry of the Ni^{II} ions is more enhanced. As far as linear trinuclear μ -phenoxy bridged Ni^{II} complexes are concerned, Ni^{II}_3 cores with coordination numbers of 4–6–4 (complex 8), 5–6–5 (complex 11), and 6–6–6 (complex 12, 13) have been reported and their exchange parameters $|J|$ are less than 10 cm^{-1} (Figures 4 and 9). The terminal Ni^{II} ions of the complex 8 are in square planar coordination geometry with a low spin state ($S = 0$), and the central Ni^{II} ion is in an axially elongated octahedral geometry with a high spin state ($S = 1$) [52]. Replacement of the ClO_4^- counter anion of 8 by Cl^- generated a linear Ni^{II}_3 complex 11 of 5(square

pyramidal)–6(octahedral)–5(square pyramidal) coordination geometry with one Cl^- anion coordinating to the axial site of each terminal Ni ion in an N_2O_2 basal plane of an analogous tetradentate ligand which has a 1,5-diazacyclooctane ring instead of the 1,4-diazacycloheptane ring of **8**. The Ni^{II}_3 complex **11** has three noninteracting high-spin Ni^{II} ions at 300 K, and weak antiferromagnetic interaction with the J_1 and J_2 values of -7.9 and -5.5 cm^{-1} , respectively, was reported [54]. Linear Ni^{II}_3 complexes with 6(octahedral)–6(octahedral)–6(octahedral) coordination geometry of noninteracting high-spin Ni^{II} ions were reported. An exchange parameter ($J_1 = 4.31 \text{ cm}^{-1}$) suggesting a weak ferromagnetic coupling was reported for complex **12** with additional μ_2 -1,3-acetato bridges between the terminal Ni ion and the central Ni ion [55]. A very weak antiferromagnetic interaction ($J_1 = -1.7 \text{ cm}^{-1}$) was reported for complex **13** of structurally similar coordination geometry to **12** [56]. The magnetic interaction of (S)-**6a** is much stronger than that of these linear trinuclear Ni^{II} complexes [25–30,54–58], which may be attributed to the unique coordination geometry in the terminal Ni^{II} ions of (S)-**6a**.

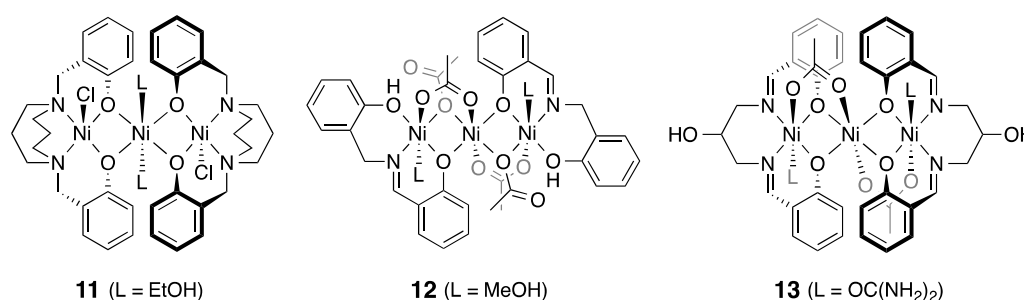


Figure 9. Trinuclear Ni complexes of 5–6–5 and 6–6–6 coordination geometry.

3.5. Reversible Coordination at Apical Sites of the Trinuclear Complexes

A large number of trinuclear complexes of general formula $(\text{L})\text{M}(\mu\text{-OR})_2\text{M}(\mu\text{-OR})_2\text{M}(\text{L})$ are known, and their solid-state chemistry is well documented as noted above. However, study on the solution chemistry of these multinuclear complexes is quite limited, probably because of their reversible decomposition into mononuclear complexes in solution [33,67]. The present M^{II}_3 complexes protected by the rigid macrocycle ligand are expected to show well-defined coordination chemistry without decomposition of the $\text{M}^{\text{II}}_3\text{O}_4$ core. In fact, it was found that the $\text{M}^{\text{II}}_3\text{O}_4$ core is stable even in the presence of a large excess amount of strongly coordinating external ligand molecules. Addition of butylamine to the Cu_3 complex (S)-**5a** in CDCl_3 caused chemical shift changes while keeping a D_2 symmetric spectral pattern (Figure 10). The pyrrole β -methyl proton signal (16- CH_3 in Scheme 2) shifted from 7.81 ppm to 11.66 ppm at 253 K. Signals of (S)-**5a** got broader at 0.5 equivalents of butylamine probably due to fast ligand exchange. Then, a single set of signals appeared at two equivalents of butylamine. The CD titration of (S)-**5a** with butylamine in CH_2Cl_2 at 25 °C showed a parabola-type titration curve that led to the association constant $K = 3.2 \times 10^3 \text{ M}^{-1}$ on the basis of fitting with a one-to-one binding isotherm (Figure S11, Supplementary Materials). This coordination behavior of (S)-**5a** with butylamine is consistent with the X-ray structure having one apical water ligand at the central Cu^{II} ion. Therefore, it is reasonably assumed that butylamine reversibly binds to either one of the apical sites of the central Cu^{II} ion (Scheme 3).

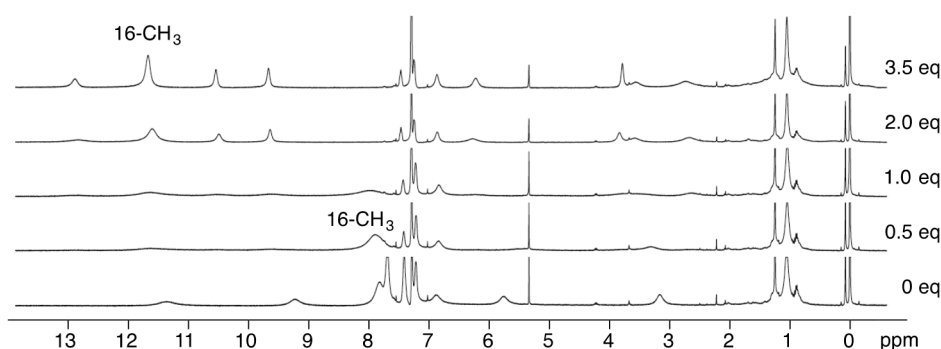
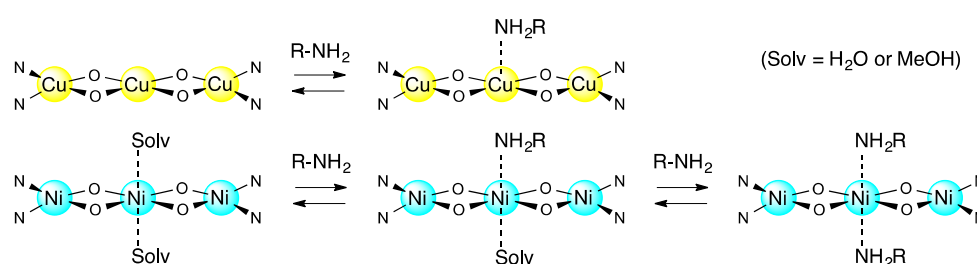


Figure 10. $^1\text{H-NMR}$ titration of (*S*)-**5a** with 0.5, 1.0, 2.0, and 3.5 equivalents of butylamine at 253 K in CDCl_3 (reproduced from the preliminary communication [17]).



Scheme 3. Coordination equilibria of (*S*)-**5a** and (*S*)-**6a** with butylamine ($\text{R} = \text{butyl}$).

UV–vis titration of the Ni_3 complex (*S*)-**6a** with 0–2.5 equivalents of butylamine showed very subtle spectral changes (Figure S12, Supplementary Materials). $^1\text{H-NMR}$ titration showed that two signals at 9.2 and 10.5 ppm due to the naphthyl protons of (*S*)-**6a** split into four signals that were finally replaced by two signals at 8.3 and 10.2 ppm when 2 equivalents of butylamine were added (Figure 11). Meanwhile, the signal at 0.60 ppm due to the methyl protons of the pyrrole β -ethyl group of (*S*)-**6a** changed to a pair of signals at 0.74 and 0.48 ppm and finally to a single signal at 0.41 ppm. These changes of the splitting pattern from D_2 to C_2 symmetry and then from C_2 to D_2 symmetry again are consistent with the stepwise binding of two butylamine ligands to the apical sites of the central Ni^{II} ion (Scheme 3). Thus, butylamine coordination to Ni^{II} is much stronger than to Cu^{II} in CH_2Cl_2 , and it is reasonably considered that (*S*)-**6a** contains two methanol ligands when precipitated from methanol.

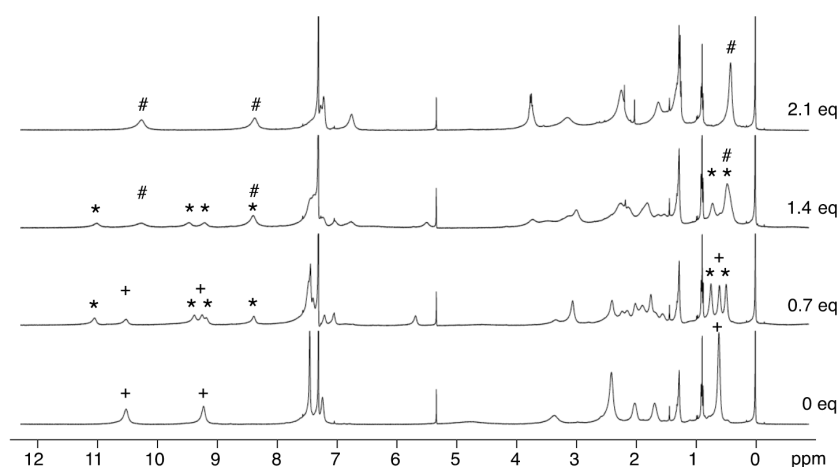


Figure 11. $^1\text{H-NMR}$ titration of (*S*)-**6a** with 0.7, 1.4, and 2.1 equivalents of butylamine at 293 K in CDCl_3 . Signals marked (+), (*), and (#) are associated with (*S*)-**6a**, (*S*)-**6a**(BuNH_2), and (*S*)-**6a**(BuNH_2)₂, respectively.

4. Conclusions

A 1,1'-bi-2-naphthol unit was embedded in a porphyrinoid macrocycle without reducing optical purity of the original 1,1'-bi-2-naphthol. The macrocycle core made of sp^2 carbons was relatively rigid and its unidirectional overall helical conformation was stable. This porphyrinoid ligand was preorganized for the linear array of three metal ions in the form of $(L)M(\mu-OR)_2M(\mu-OR)_2M(L)$. X-ray crystallography of the Cu^{II}_3 complex showed that a pair of very planar Cu_2O_2 cores was only slightly off coplanarity (plane-to-plane angle 8.3°), and the terminal Cu ions were highly distorted from square planar geometry. 1H -NMR study on the Cu^{II}_3 complex revealed unusual temperature dependency of the chemical shifts of the naphthyl protons, which were indicative of the strong antiferromagnetic coupling between the Cu atoms. The observed paramagnetic shifts in the pyrrolic ligand and the binaphthyl ligand could be used to estimate spin delocalization from the terminal metal and the central metal, respectively, and these paramagnetic 1H -NMR data were consistent with the spin densities calculated via DFT using $\omega B97XD$ functional. The strong antiferromagnetic coupling observed for both Cu^{II}_3 ($J = -434 \text{ cm}^{-1}$) and Ni^{II}_3 ($J = -49 \text{ cm}^{-1}$) complexes could be ascribed to the unique coordination geometry that was also responsible for reversible ligation of butylamine only at the central metal ion without decomposition of the trinuclear core. This apical ligand binding could be studied using well-resolved 1H -NMR spectra of both Cu^{II}_3 and Ni^{II}_3 complexes. The present multinuclear complexes of an enantiomerically pure helical porphyrin analogue are expected to lead to further exploration of the interesting chemistry of helical multinuclear complexes.

Supplementary Materials: The following are available online at <http://www.mdpi.com/2073-8994/12/10/1610/s1>: Figure S1. 1H -NMR spectra of (S)-3,3'-bis(5-carboethoxy-4-ethyl-3-methyl-2-pyrrolyl)-1,1'-bi-2-naphthol ((S)-**2a**) and (S)-3,3'-bis(5-carboethoxy-3,4-diethyl-2-pyrrolyl)-1,1'-bi-2-naphthol ((S)-**2b**); Figure S2. 1H -NMR spectra of (S)-3,3'-bis(4-ethyl-3-methyl-2-pyrrolyl)-1,1'-bi-2-naphthol ((S)-**3a**) and (S)-3,3'-bis(3,4-diethyl-2-pyrrolyl)-1,1'-bi-2-naphthol ((S)-**3b**); Figure S3. 1H -NMR spectra of the bis(binaphthol)tetrapyrrole (S)-**4a** and (S)-**4b**; Figure S4. Variable-temperature 1H -NMR spectra of the Cu_3 complex of bis(binaphthol)tetrapyrrole ((S)-**5a**); Figure S5. Variable-temperature 1H NMR spectra of the Cu_3 complex of bis(binaphthol)tetrapyrrole ((S)-**5b**); Figure S6. Variable-temperature 1H NMR spectra of the Ni_3 complex of bis(binaphthol)tetrapyrrole ((S)-**6a**); Figure S7. Variable-temperature 1H NMR spectra of the Ni_3 complex of bis(binaphthol)tetrapyrrole ((S)-**6b**); Figure S8. 2D COSY spectrum of the Cu_3 complex of bis(binaphthol)tetrapyrrole ((S)-**5a**) at 313 K; Figure S9. 2D COSY spectrum of the Ni_3 complex of bis(binaphthol)tetrapyrrole ((S)-**6a**) at 293 K; Figure S10. CD spectra of (R)-**4a** and (S)-**4a** in CH_2Cl_2 and their HPLC traces on a chiral column; Figure S11. CD and UV-vis spectral changes of (S)-**5a** upon addition of butylamine in CH_2Cl_2 ; Figure S12. CD and UV-Vis spectral changes of (S)-**6a** in CH_2Cl_2 upon addition of butylamine; Figure S13. DFT-calculated structure of (S)-**5a** of doublet and quartet using B3LYP functional and $\omega B97XD$ functional; Table S1. Cu-to-H distances (\AA) in the X-ray structure of (S)-**5a**; Table S2. Structural data (distance (\AA) and angle ($^\circ$)) of the Cu_3O_4 core of (S)-**5a** obtained by X-ray crystallography and theoretical DFT calculations; Table S3. Spin density of (S)-**5a** calculated by DFT (6-31G(d), LANL2DZ/ $\omega B97XD$); Table S4. Spin density of (S)-**5a** calculated by DFT (6-31G(d), LANL2DZ/B3LYP).

Author Contributions: Conceptualization, J.-i.S.; validation, J.-i.S.; formal analysis, S.O., Y.T., T.S., and T.M.; investigation, S.O., Y.T., and T.S.; resources, J.-i.S., T.S., and H.O.; data curation, J.-i.S. and T.S.; writing—original draft preparation, J.-i.S.; writing—review and editing, J.-i.S., T.M., and H.O.; visualization, J.-i.S.; supervision, J.-i.S.; project administration, J.-i.S.; funding acquisition, J.-i.S. All authors read and agreed to the published version of the manuscript.

Funding: This research was funded by the Japan Society of Promotion of Science (JSPS), grant number (21550045) and the Hyogo Science and Technology Association Japan, grant number (211068).

Conflicts of Interest: The authors declare no conflict of interest.

References

1. Sessler, J.L.; Tomat, E. Transition-metal Complexes of Expanded Porphyrins. *Acc. Chem. Res.* **2007**, *40*, 371–379. [[CrossRef](#)] [[PubMed](#)]
2. Shimizu, S.; Osuka, A. Metalation Chemistry of *meso*-Aryl-Substituted Expanded Porphyrins. *Eur. J. Inorg. Chem.* **2006**, *2006*, 1319–1335. [[CrossRef](#)]
3. Vogel, E. Novel Porphyrinoid Macrocycles and Their Metal Complexes. *J. Heterocycl. Chem.* **1996**, *33*, 1461–1487. [[CrossRef](#)]

4. Weghorn, S.J.; Sessler, J.L.; Lynch, V.; Baumann, T.F.; Sibert, J.W. Bis[(μ -chloro)copper(II)] Amethyrin: A Bimetallic Copper(II) Complex of an Expanded Porphyrin. *Inorg. Chem.* **1996**, *35*, 1089–1090. [[CrossRef](#)]
5. Shimizu, S.; Anand, V.G.; Taniguchi, R.; Furukawa, K.; Kato, T.; Yokoyama, T.; Osuka, A. Biscopper Complexes of *meso*-Alkyl-Substituted Hexaphyrin: Gable Structures and Varying Antiferromagnetic Coupling. *J. Am. Chem. Soc.* **2004**, *126*, 12280–12281. [[CrossRef](#)]
6. Frensch, L.K.; Proepper, K.; John, M.; Demeshko, S.; Brueckner, C.; Meyer, F. Siamese-Twin Porphyrins: A Pyrazole-Based Expanded Porphyrin Providing a Bimetallic Cavity. *Angew. Chem.* **2011**, *123*, 1456–1460; *Angew. Chem. Int. Ed.* **2011**, *50*, 1420–1424. [[CrossRef](#)]
7. Givaja, G.; Volpe, M.; Leeland, J.W.; Edwards, M.A.; Young, T.K.; Darby, S.B.; Reid, S.D.; Blake, A.J.; Wilson, C.; Wolowska, J.E.; et al. Design and Synthesis of Binucleating Macrocyclic Clefs Derived from Schiff-Base Calixpyrroles. *Chem. Eur. J.* **2007**, *13*, 3707–3723. [[CrossRef](#)]
8. Veauthier, J.M.; Tomat, E.; Lynch, V.M.; Sessler, J.L.; Mirsaidov, U.; Markert, J.T. Calix[4]pyrrole Schiff Base Macrocycles: Novel Binucleating Ligands for Cu(I) and Cu(II). *Inorg. Chem.* **2005**, *44*, 6736–6743. [[CrossRef](#)]
9. Volpe, M.; Hartnett, H.; Leeland, J.W.; Wills, K.; Ogunshun, M.; Duncombe, B.J.; Wilson, C.; Blake, A.J.; McMaster, J.; Love, J.B. Binuclear Cobalt Complexes of Schiff-Base Calixpyrroles and Their Roles in the Catalytic Reduction of Dioxygen. *Inorg. Chem.* **2009**, *48*, 5195–5207. [[CrossRef](#)]
10. Askarizadeh, E.; Yaghoob, S.B.; Boghaei, D.M.; Slawin, A.M.Z.; Love, J.B. Tailoring Dicobalt Pacman Complexes of Schiff-base Calixpyrroles towards Dioxygen Reduction Catalysis. *Chem. Commun.* **2010**, *46*, 710–712. [[CrossRef](#)]
11. Kamimura, Y.; Shimizu, S.; Osuka, A. [40] Nonaphyrin(1.1.1.1.1.1.1.1) and Its Heterometallic Complexes with Palladium–Carbon Bonds. *Chem. Eur. J.* **2007**, *13*, 1620–1628. [[CrossRef](#)] [[PubMed](#)]
12. Inoue, M.; Ikeda, C.; Kawata, Y.; Venkatraman, S.; Furukawa, K.; Osuka, A. Synthesis of Calix [3]dipyrins by a Modified Lindsey Protocol. *Angew. Chem.* **2007**, *119*, 2356–2359; *Angew. Chem. Int. Ed.* **2007**, *46*, 2306–2309. [[CrossRef](#)]
13. Yoneda, T.; Sung, Y.M.; Lim, J.M.; Kim, D.; Osuka, A. Pd^{II} Complexes of [44]- and [46] Decaphyrins: The Largest Hückel Aromatic and Antiaromatic, and Möbius Aromatic Macrocycles. *Angew. Chem. Int. Ed.* **2014**, *53*, 13169–13173. [[CrossRef](#)]
14. Soya, T.; Naoda, K.; Osuka, A. Ni^{II} Metallations of [40]- and [42] Nonaphyrins(1.1.1.1.1.1.1.1): The Largest Doubly Twisted Hückel Antiaromatic Molecule. *Chem. Asian J.* **2015**, *10*, 231–238. [[CrossRef](#)] [[PubMed](#)]
15. Setsune, J.; Toda, M.; Yoshida, T. Synthesis and Dynamic Structure of Multinuclear Rh Complexes of Porphyrinoids. *Chem. Commun.* **2008**, 1425–1428. [[CrossRef](#)] [[PubMed](#)]
16. Setsune, J.; Toda, M.; Yoshida, T.; Imamura, K.; Watanabe, K. The Synthesis and Dynamic Structures of Multinuclear Complexes of Large Porphyrinoids Expanded by Phenylene and Thienylene Spacers. *Chem. Eur. J.* **2015**, *21*, 12715–12727. [[CrossRef](#)]
17. Setsune, J.; Omae, S. Homohelical Porphyrin Analogue Embedded with Binaphthol Units. *Chem. Lett.* **2012**, *41*, 168–169. [[CrossRef](#)]
18. Ferguson, G.; Langrick, C.R.; Parker, D.; Matthes, K.E. A Linear Trinuclear Macrocyclic Copper(II) Complexes. *J. Chem. Soc. Chem. Commun.* **1985**, *22*, 1609–1610. [[CrossRef](#)]
19. Cronin, L.; Walton, P.H. Synthesis and Single Crystal X-ray Structure of a Novel Trinuclear Copper(II) Methoxide Complex. *Inorg. Chim. Acta* **1998**, *269*, 241–245. [[CrossRef](#)]
20. Ruf, M.; Pierpont, C.G. Methoxide Coordination at the Pocket of [Cu^{II}Tp^{Cum}·Me] and a Simple Model for the Center of Galactose Oxidase. *Angew. Chem.* **1998**, *110*, 1830–1832; *Angew. Chem. Int. Ed.* **1998**, *37*, 1736–1739. [[CrossRef](#)]
21. Shakya, R.; Jozwiuk, A.; Powell, D.R.; Houser, R.P. Synthesis and Characterization of Polynuclear Copper(II) Complexes with Pyridylbis(phenol) Ligands. *Inorg. Chem.* **2009**, *48*, 4083–4088. [[CrossRef](#)] [[PubMed](#)]
22. Barta, C.A.; Bayly, S.R.; Read, P.W.; Patrick, B.O.; Thompson, R.C.; Orvig, C. Molecular Architectures for Trimetallic d/f/d Complexes: Magnetic Studies of a LnCu₂ Core. *Inorg. Chem.* **2008**, *47*, 2294–2302. [[CrossRef](#)] [[PubMed](#)]
23. Song, Y.-F.; van Albada, G.A.; Tang, J.; Mutikainen, I.; Turpeinen, U.; Massera, C.; Roubeau, O.; Costa, J.S.; Gamez, P.; Reedijk, J. Controlled Copper-Mediated Chlorination of Phenol Rings under Mild Conditions. *Inorg. Chem.* **2007**, *46*, 4944–4950. [[CrossRef](#)] [[PubMed](#)]

24. Thakurta, S.; Chakraborty, J.; Rosair, G.; Tercero, J.; El Fallah, M.S.; Garribba, E.; Mitra, S. Synthesis of Two New Linear Trinuclear Cu^{II} Complexes: Mechanism of Magnetic Coupling through Hybrid B3LYP Functional and CShM Studies. *Inorg. Chem.* **2008**, *47*, 6227–6235. [[CrossRef](#)]
25. Blake, A.J.; Brechin, E.K.; Codron, A.; Gould, R.O.; Grant, C.M.; Parsons, S.; Rawson, J.M.; Winpenny, R.E.P. New Polynuclear Nickel Complexes with a Variety of Pyridonate and Carboxylate Ligands. *J. Chem. Soc. Chem. Commun.* **1995**, *19*, 1983–1985. [[CrossRef](#)]
26. Kavlakoglu, E.; Elmali, A.; Elerman, Y.; Werner, R.; Svoboda, I.; Fuess, H. Crystal Structure and Magnetic Properties of a Linear Trinuclear Ni(II) Complex. *Z. Naturforsch. B Chem. Sci.* **2001**, *56*, 43–48. [[CrossRef](#)]
27. Banerjee, S.; Drew, M.G.B.; Lu, C.-Z.; Tercero, J.; Diaz, C.; Ghosh, A. Dinuclear Complexes of M^{II} Thiocyanate (M = Ni and Cu) Containing a Tridentate Schiff-Base Ligand: Synthesis, Structural Diversity and Magnetic Properties. *Eur. J. Inorg. Chem.* **2005**, *12*, 2376–2383. [[CrossRef](#)]
28. Sharma, A.K.; Lloret, F.; Mukherjee, R. Phenolate and Acetate (Both μ_2 -1,1 and μ_2 -1,3 Mode)-Bridged Face-Shared Trioctahedral Linear Ni^{II}₃, Ni^{II}₂M^{II} (M = Mn, Co) Complexes: Ferro- and Antiferromagnetic Coupling. *Inorg. Chem.* **2007**, *46*, 5128–5130. [[CrossRef](#)]
29. Beissel, T.; Birkelbach, F.; Bill, E.; Glaser, T.; Kesting, F.; Krebs, C.; Weyhermüller, T.; Wieghardt, K.; Butzlaff, C.; Trautwein, A.X. Exchange and Double-Exchange Phenomena in Linear Homo- and Heterotrinary Nickel (II,III,IV) Complexes Containing Six μ_2 -Phenolato or μ_2 -Thiophenolato Bridging Ligand. *J. Am. Chem. Soc.* **1996**, *118*, 12376–12390. [[CrossRef](#)]
30. Xu, Z.; Thompson, L.K.; Milway, V.A.; Zhao, L.; Kelly, T.; Miller, D.O. Self-Assembled Dinuclear, Trinuclear, Tetranuclear, Pentanuclear, and Octanuclear Ni(II) Complexes of a Series of Polytopic Diazine Based Ligands: Structural and Magnetic Properties. *Inorg. Chem.* **2003**, *42*, 2950–2959. [[CrossRef](#)]
31. Fontecha, J.B.; Goetz, S.; McKee, V. Di-, Tri-, and Tetracopper(II) Complexes of a Pseudocalixarene Macrocyclic. *Angew. Chem.* **2002**, *114*, 4735–4738; *Angew. Chem. Int. Ed.* **2002**, *41*, 4553–4556. [[CrossRef](#)]
32. Esteves, C.V.; Mateus, P.; André, V.; Bandeira, N.A.G.; Calhorda, M.J.; Ferreira, L.P.; Delgado, R. Di-versus Trinuclear Copper(II) Cryptate for the Uptake of Dicarboxylate Anions. *Inorg. Chem.* **2016**, *55*, 7051–7060. [[CrossRef](#)] [[PubMed](#)]
33. Izzet, G.; Akdas, H.; Hucher, N.; Giorgi, M.; Prange, T.; Reinaud, O. Supramolecular Assemblies with Calix[6]arenes and Copper Ions: From Dinuclear to Trinuclear Linear Arrangements of Hydroxo-Cu(II) Complexes. *Inorg. Chem.* **2006**, *45*, 1069–1077. [[CrossRef](#)] [[PubMed](#)]
34. Beer, G.; Niederaalt, C.; Grimme, S.; Daub, J. Redox Switches with Chiroptical Signal Expression Based on Binaphthyl Boron Dipyrromethene Conjugates. *Angew. Chem.* **2000**, *112*, 3385–3388; *Angew. Chem. Int. Ed.* **2000**, *39*, 3252–3255. [[CrossRef](#)]
35. Al-Sheikh-Ali, A.; Benson, R.E.; Blumentritt, S.; Cameron, T.S.; Linden, A.; Wolstenholme, D.; Thompson, A. Asymmetric Synthesis of Mono- and Dinuclear Bis(dipyrinato) Complexes. *J. Org. Chem.* **2007**, *72*, 4947–4952.
36. Gunst, K.; Seggewies, S.; Breitmaier, E. New Chiral Macrocyclic Di-imines Containing Tetrapyrrole and Tripyrrane Subunits. *Synthesis* **2001**, *12*, 1856–1860. [[CrossRef](#)]
37. Miyaji, H.; Hong, S.-J.; Jeong, S.-D.; Yoon, D.-W.; Na, H.-K.; Hong, J.; Ham, S.; Sessler, J.L.; Lee, C.-H. A Binol-Strapped Calix[4]pyrrole as a Model Chirogenic Receptor for the Enantioselective Recognition of Carboxylate Anions. *Angew. Chem.* **2007**, *119*, 2560–2563; *Angew. Chem. Int. Ed.* **2007**, *46*, 2508–2511. [[CrossRef](#)]
38. Setsune, J.; Toda, M.; Watanabe, K.; Panda, P.K.; Yoshida, T. Synthesis of Bis(pyrrol-2-yl)arenes by Pd-Catalyzed Cross Coupling. *Tetrahedron Lett.* **2006**, *47*, 7541–7544.
39. Setsune, J.; Watanabe, K. Cryptand-like Porphyrinoid Assembled with Three Dipyrpyridine Chains: Synthesis, Structure, and Homotropic Positive Allosteric Binding of Carboxylic Acids. *J. Am. Chem. Soc.* **2008**, *130*, 2404–2405. [[CrossRef](#)]
40. Sheldrick, G.M. *SHELXTL 5.10 for Windows NT: Structure Determination Software Programs*; Bruker Analytical X-ray Systems, Inc.: Madison, WI, USA, 1997.
41. Bain, G.A.; Bery, J.E. Diamagnetic Corrections and Pascal's Constants. *J. Chem. Educ.* **2008**, *85*, 532. [[CrossRef](#)]
42. Frisch, M.J.; Trucks, G.W.; Schlegel, H.B.; Scuseria, G.E.; Robb, M.A.; Cheeseman, J.R.; Scalmani, G.; Barone, V.; Mennucci, B.; Petersson, G.A.; et al. *Gaussian 09, Revision C.01*; Gaussian, Inc.: Wallingford, CT, USA, 2009.
43. Wu, T.R.; Shen, L.; Chong, J.M. Asymmetric Allylboration of Aldehyde and Ketones Using 3,3'-Disubstitutedbinaphthol-Modified Boronates. *Org. Lett.* **2004**, *6*, 2701–2704. [[CrossRef](#)] [[PubMed](#)]

44. Suresh, P.; Srimurugan, S.; Babu, B.; Pati, H.N. Synthesis of Some Acetylene-Tethered Chiral and Achiral Dialdehydes. *Acta Chim. Slov.* **2008**, *55*, 453–457.
45. Kudo, N.; Perseghini, M.; Fu, G.C. A Versatile Method for Suzuki Cross-Coupling Reactions of Nitrogen Heterocycles. *Angew. Chem.* **2006**, *118*, 1304–1306; *Angew. Chem. Int. Ed.* **2006**, *45*, 1282–1284. [[CrossRef](#)]
46. Fu, G.C. The Development of Versatile Methods for Palladium-Catalyzed Coupling Reactions of Aryl Electrophiles through the Use of P(*t*-Bu)₃ and PCy₃ as Ligands. *Acc. Chem. Res.* **2008**, *41*, 1555–1564. [[CrossRef](#)] [[PubMed](#)]
47. Rothmund, P.A. New Porphyrin Synthesis. The Synthesis of Porphin. *J. Am. Chem. Soc.* **1936**, *58*, 625–627. [[CrossRef](#)]
48. Song, Y.; Gamez, P.; Roubeau, O.; Lutz, M.; Spek, A.L.; Reedijk, J. Structural and Magnetic Characterization of a Linear Trinuclear Copper Complex Formed through Ligand Sharing. *Eur. J. Inorg. Chem.* **2003**, *16*, 2924–2928. [[CrossRef](#)]
49. Song, Y.; Gamez, P.; Roubeau, O.; Mutikainen, I.; Turpeinen, U.; Reedijk, J. Structure and Magnetism of Two New Linear Trinuclear Copper(II) Clusters Obtained from the Tetradentate N₂O₂ Ligand Bis(2-hydroxybenzyl)-1,3-diaminopropane. *Inorg. Chim. Acta* **2005**, *358*, 109–115. [[CrossRef](#)]
50. Song, Y.; van Albada, G.A.; Quesada, M.; Mutikainen, I.; Turpeinen, U.; Reedijk, J. A New Linear Trinuclear Cu(II) Complex [Cu₃L₂(MeCN)₂L₂](MeCN)₂ with Semi-Coordinated Iodides Formed through Ligand Sharing (H₂L = 1,7-Bis(2-hydroxyphenyl)-2,6-diaza-4-hydroxyl-heptane). *Inorg. Chem. Commun.* **2005**, *8*, 975–978. [[CrossRef](#)]
51. Bu, W.-H.; Du, M.; Shang, Z.-L.; Zhang, R.-H.; Liao, D.-Z.; Shionoya, M.; Clifford, T. Varying Coordination Modes and Magnetic Properties of Copper(II) Complexes with Diazamesocyclic Ligands by Altering Additional Donor Pendants on 1,5-Diazacyclooctane. *Inorg. Chem.* **2000**, *39*, 4190–4199. [[CrossRef](#)]
52. Du, M.; Zhao, X.-J.; Guo, J.-H.; Bu, X.-H.; Ribas, J. Towards the Design of Linear Homo-Trinuclear Metal Complexes Based on a New Phenol-Functionalised Diazamesocyclic Ligand: Structural Analysis and Magnetism. *Eur. J. Inorg. Chem.* **2005**, *2*, 294–304. [[CrossRef](#)]
53. Epstein, J.M.; Figgis, B.N.; White, A.H.; Willis, A.C. Crystal Structures of Two Trinuclear Schiff-Based Copper(II) Complexes. *J. Chem. Soc. Dalton Trans.* **1974**, 1954–1961. [[CrossRef](#)]
54. Bu, X.-H.; Du, M.; Zhang, L.; Liao, D.-Z.; Tang, J.-K.; Zhang, R.-H.; Shionoya, M. Novel Nickel(II) Complexes with Diazamesocyclic Ligands Functionalized by Additional Phenol Donor Pendant(s): Synthesis, Characterization, Crystal Structures and Magnetic Properties. *J. Chem. Soc. Dalton Trans.* **2001**, 593–598. [[CrossRef](#)]
55. Wang, Q.-L.; Yang, C.; Qi, L.; Liao, D.-Z.; Yang, G.-M.; Ren, H.-X. A Trinuclear Nickel(II) Complex with Dissimilar Bridges: Synthesis, Crystal Structure, Spectroscopy and Magnetism. *J. Mol. Struct.* **2008**, *892*, 88–92. [[CrossRef](#)]
56. Lu, J.-W.; Chen, C.-Y.; Kao, M.-C.; Cheng, C.-M.; Wei, H.-H. Synthesis, Crystal Structure, and Magnetic Properties of μ -Phenoxo/ μ -Carboxylato-Bridged Trinuclear Nickel(II) Complexes with Schiff Base, DMF, and Urea Ligands. *J. Mol. Struct.* **2009**, *936*, 228–233. [[CrossRef](#)]
57. Mukherjee, P.; Drew, M.G.B.; Gomez-Garcia, C.J.; Ghosh, A. (Ni₂), (Ni₃), and (Ni₂ + Ni₃): A Unique Example of Isolated and Cocrystallized Ni₂ and Ni₃ Complexes. *Inorg. Chem.* **2009**, *48*, 4817–4827. [[CrossRef](#)]
58. Zhang, L.; Gao, W.; Wu, Q.; Su, Q.; Zhang, J.; Mu, Y. Synthesis and Characterization of Chiral Trinuclear Cobalt and Nickel Complexes Supported by Binaphthol-derived Bis(salicylaldimine) Ligands. *J. Coord. Chem.* **2013**, *66*, 3182–3192. [[CrossRef](#)]
59. Evans, D.F. The Determination of the Paramagnetic Susceptibility of Substances in Solution by Nuclear Magnetic Resonance. *J. Chem. Soc.* **1959**, 2003–2005. [[CrossRef](#)]
60. Schubert, E.M. Utilizing the Evans Method with a Superconducting NMR Spectrometer in the Undergraduate Laboratory. *J. Chem. Educ.* **1992**, *69*, 62. [[CrossRef](#)]
61. Grant, D.H. Paramagnetic Susceptibility by NMR: The “Solvent Correction” Reexamined. *J. Chem. Educ.* **1995**, *72*, 39–40. [[CrossRef](#)]
62. Bertini, I.; Luchinat, C. NMR of Paramagnetic Substances. *Coord. Chem. Rev.* **1996**, *150*, 1–296.
63. Bren, K.L. NMR Analysis of Spin States and Spin Densities. In *Spin States in Biochemistry and Inorganic Chemistry: Influence on Structure and Reactivity*; Swart, M., Costas, M., Eds.; Wiley: Chichester, UK, 2016; Volume 16, pp. 409–434.
64. Kahn, O. *Molecular Magnetism*; VCH: New York, NY, USA, 1993.

65. Thompson, L.K.; Mandal, S.K.; Tandon, S.S.; Bridson, J.N.; Park, M.K. Magnetostructural Correlations in Bis(μ_2 -phenoxide)-Bridged Macrocyclic Dinuclear Copper(II) Complexes. Influence of Electron-Withdrawing Substituents on Exchange Coupling. *Inorg. Chem.* **1996**, *35*, 3117–3125. [[CrossRef](#)] [[PubMed](#)]
66. Nanda, K.K.; Das, R.; Thompson, L.K.; Venkatsubramanian, K.; Paul, P.; Nag, K. Magneto-Structural Correlations in Macrocyclic Dinickel(II) Complexes: Tuning of Spin Exchange by Varying Stereochemistry and Auxiliary Ligands. *Inorg. Chem.* **1994**, *33*, 1188–1193. [[CrossRef](#)]
67. Carbonaro, L.; Isola, M.; La Pegna, P.; Senatore, L.; Marchetti, F. Spectrophotometric Study of the Equilibria between Nickel(II) Schiff-Base Complexes and Alkaline Earth or Nickel(II) Cations in Acetonitrile Solution. *Inorg. Chem.* **1999**, *38*, 5519–5525. [[CrossRef](#)] [[PubMed](#)]



© 2020 by the authors. Licensee MDPI, Basel, Switzerland. This article is an open access article distributed under the terms and conditions of the Creative Commons Attribution (CC BY) license (<http://creativecommons.org/licenses/by/4.0/>).